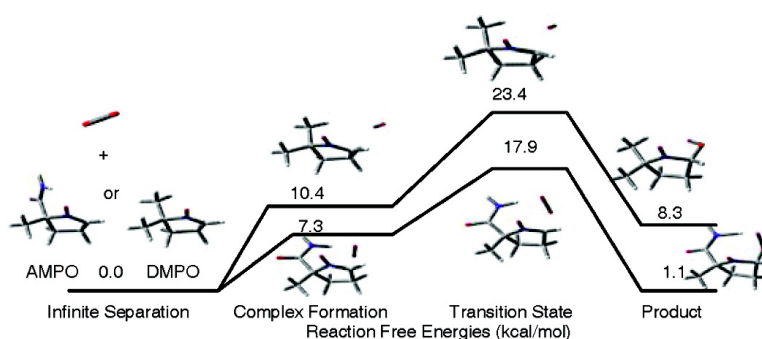


Reactivity of Superoxide Radical Anion with Cyclic Nitrones: Role of Intramolecular H-Bond and Electrostatic Effects

Frederick A. Villamena, Shijing Xia, John K. Merle, Robert Lauricella,
 Beatrice Tuccio, Christopher M. Hadad, and Jay L. Zweier

J. Am. Chem. Soc., **2007**, 129 (26), 8177-8191 • DOI: 10.1021/ja0702622 • Publication Date (Web): 12 June 2007

Downloaded from <http://pubs.acs.org> on February 16, 2009



More About This Article

Additional resources and features associated with this article are available within the HTML version:

- Supporting Information
- Links to the 8 articles that cite this article, as of the time of this article download
- Access to high resolution figures
- Links to articles and content related to this article
- Copyright permission to reproduce figures and/or text from this article

[View the Full Text HTML](#)



Reactivity of Superoxide Radical Anion with Cyclic Nitrones: Role of Intramolecular H-Bond and Electrostatic Effects

Frederick A. Villamena,^{*,†,‡} Shijing Xia,[§] John K. Merle,[§] Robert Lauricella,^{||}
Beatrice Tuccio,^{||} Christopher M. Hadad,^{*,§} and Jay L. Zweier^{*,‡}

Contribution from the Department of Pharmacology, Center for Biomedical EPR Spectroscopy and Imaging, The Davis Heart and Lung Research Institute, and the Division of Cardiovascular Medicine, Department of Internal Medicine, College of Medicine, and Department of Chemistry, The Ohio State University, Columbus, Ohio 43210, and Laboratory TRACES, JE 2421, Aix-Marseille Universite, Faculte St. Jerome, 13397 Marseille cedex 20, France

Received January 12, 2007; E-mail: Frederick.Villamena@osumc.edu; hadad.1@osu.edu; Jay.Zweier@osumc.edu

Abstract: Limitations exist among the commonly used cyclic nitron spin traps for biological free radical detection using electron paramagnetic resonance (EPR) spectroscopy. The design of new spin traps for biological free radical detection and identification using EPR spectroscopy has been a major challenge due to the lack of systematic and rational approaches to their design. In this work, density functional theory (DFT) calculations and stopped-flow kinetics were employed to predict the reactivity of functionalized spin traps with superoxide radical anion ($O_2^{\bullet-}$). Functional groups provide versatility and can potentially improve spin-trap reactivity, adduct stability, and target specificity. The effect of functional group substitution at the C-5 position of pyrroline *N*-oxides on spin-trap reactivity toward $O_2^{\bullet-}$ was computationally rationalized at the PCM/B3LYP/6-31+G(d,p)/B3LYP/6-31G(d) and PCM/mPW1K/6-31+G(d,p) levels of theory. Calculated free energies and rate constants for the reactivity of $O_2^{\bullet-}$ with model nitrones were found to correlate with the experimentally obtained rate constants using stopped-flow and EPR spectroscopic methods. New insights into the nucleophilic nature of $O_2^{\bullet-}$ addition to nitrones as well as the role of intramolecular hydrogen bonding of $O_2^{\bullet-}$ in facilitating this reaction are discussed. This study shows that using an *N*-monoalkylsubstituted amide or an ester as attached groups on the nitron can be ideal in molecular tethering for improved spin-trapping properties and could pave the way for improved *in vivo* radical detection at the site of superoxide formation.

1. Introduction

Nitrones are members of a class of compounds which are commonly used as precursors in the synthesis of natural products,¹ as spin-trapping reagents in the identification of transient radicals,² and as therapeutic agents^{3,4} such as in the case of disodium-[(*tert*-butylimino)-methyl]benzene-1,3-disulfonate *N*-oxide (NXY-059) which is in clinical trials in the USA for the treatment of neurodegenerative disease.⁵ In recent years, it has become clear that reactive oxygen species (ROS) (e.g., radicals: $O_2^{\bullet-}$, HO^{\bullet} , HO_2^{\bullet} , RO_2^{\bullet} , RO^{\bullet} , $CO_3^{\bullet-}$, and $CO_2^{\bullet-}$; and

nonradicals such as H_2O_2 , $HOCl$, O_3 , 1O_2 , and $ROOH$) are critical mediators in cardiovascular dysfunction, neurodegenerative diseases, oncogenesis, lung damage, and aging, to name a few.⁶ Electron paramagnetic resonance (EPR) spectroscopy has been an indispensable tool for the detection of these ROS via spin trapping.^{2,7,8} The nitron-based spin traps (Chart 1), 5,5-dimethyl-1-pyrroline *N*-oxide (DMPO), 5-diethoxyphosphoryl-5-methyl-pyrroline *N*-oxide (DEPMPO), and 5-ethoxycarbonyl-5-methyl-pyrroline *N*-oxide (EMPO), are the most commonly used spin-trapping reagents and have contributed significantly to the understanding of important free-radical-mediated processes in chemical, biochemical, and biological systems in spite of their many limitations. For example, the direct or indirect observations of $O_2^{\bullet-}/HO_2^{\bullet}$ formation have been achieved by spin trapping in the following systems: melano-

[†] Department of Pharmacology, The Ohio State University.

[‡] Davis Heart and Lung Research Institute and Department of Internal Medicine, The Ohio State University.

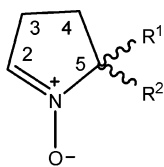
[§] Department of Chemistry, The Ohio State University.

^{||} Aix-Marseille Universite.

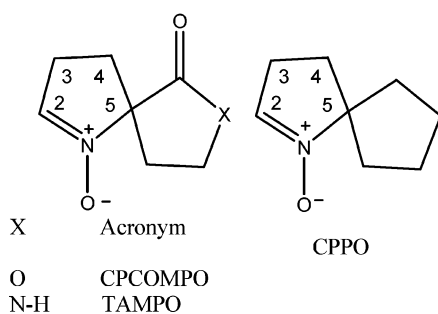
- (1) Breuer, E.; Aurich, H. G.; Nielsen, A. *Nitrones, Nitronates and Nitroxides*; John Wiley and Sons: New York, 1989. Torsell, K. B. G. *Nitrile Oxides, Nitrones, and Nitronates in Organic Synthesis*; VCH Verlagsgesellschaft mbH: Weinheim, 1988.
- (2) Villamena, F. A.; Zweier, J. L. *Antioxid. Redox Signaling* **2004**, *6*, 619–629.
- (3) Floyd, R. A.; Hensley, K. *Ann. N.Y. Acad. Sci.* **2000**, *899*, 222–237; Inanami, O.; Kuwabara, M. *Free Radical Res.* **1995**, *23*, 33–9.
- (4) *Handbook of Synthetic Antioxidants*; Packer, L., Cadenas, E., Eds.; Marcel Dekker, Inc.: New York, 1997.
- (5) Becker, D. A.; Ley, J. J.; Echegoyen, L.; Alvarado, R. *J. Am. Chem. Soc.*, **2002**, *124*, 4678. Ginsberg, M. D.; Becker, D. A.; Busto, R.; Belayev, A.; Zhang, Y.; Khoutorova, L.; Ley, J. J.; Zhao, W.; Belayev, L. *Ann. Neurol.* **2003**, *54*, 330.

- (6) Halliwell, B. *Oxidative Stress and Disease* **2001**, *7*, 1–16. Halliwell, B. *Drugs Aging* **2001**, *18*, 685–716. Zweier, J. L.; Talukder, M. A. H. *Cardiovasc. Res.* **2006**, *70*, 181–190. Zweier, J. L.; Villamena, F. A. In *Oxidative Stress and Cardiac Failure*; Kukin, M. L., Fuster, V., Eds.; Futura Publishing: Armonk, NY, 2003; pp 67–95.
- (7) Janzen, E. G. *Free Radical Biol. Med.* **1980**, *4*, 115–154. Janzen, E. G. *Acc. Chem. Res.* **1971**, *4*, 31–40. Janzen, E. G.; Haire, D. L. *Adv. Free Radical Chem.* **1990**, *1*, 253–295. Rosen, G. M.; Britigan, B. E.; Halpern, H. J.; Pou, S. *Free Radicals: Biology and Detection by Spin Trapping*; Oxford University Press: New York, 1999.
- (8) *Toxicology of the Human Environment. The Critical Role of Free Radicals*; Rhodes, C. J., Ed.; Taylor and Francis: London, 2000.

Chart 1. DMPO-Type Nitrones Used as Models for the Theoretical Investigation of Spin Trapping of Superoxide Radical Anion



R ¹	R ²	Acronym
-CH ₃	-CH ₃	DMPO
-CH ₃	-CF ₃	TFMPO
-CH ₃	-C(O)NH ₂	AMPO
-CH ₃	-C(O)NHCH ₃	MAMPO
-CH ₃	-C(O)N(CH ₃) ₂	DiMAMPO
-CH ₃	-CO ₂ Et	EMPO
-CH ₃	-P(O)(OEt) ₂	DEPMPO
-CO ₂ Et	-CO ₂ Et	DEPO
-CO ₂ Et	-C(O)NHCH ₃	EMAPO
-C(O)NHCH ₃	-C(O)NHCH ₃	DiMAPO



somes,⁹ mitochondria,¹⁰ photosynthetic systems,¹¹ nitric oxide synthase (NOS),¹² endothelial cells,¹³ human neutrophils,¹⁴ and reperused heart tissue.¹⁵ Moreover, EPR spin trapping has been employed in the understanding of radical-mediated mechanisms in the fields of fuel cell technology,¹⁶ nanomaterials,¹⁷ photodynamic therapy,¹⁸ environmental remediation,¹⁹ and simple organic transformations.²⁰

- (9) Zareba, M.; Szweczyk, G.; Sarna, T.; Hong, L.; Simon, J. D.; Henry, M. M.; Burke, J. M. *Photochem. Photobiol.* **2006**, *82*, 1024–1029.
- (10) Chen, Y.-R.; Chen, C.-L.; Yeh, A.; Liu, X.; Zweier, J. L. *J. Biol. Chem.* **2006**, *281*, 13159–13168. Dugan, L. L.; Sensi, S. L.; Canzoniero, L. M. T.; Handran, S. D.; Rothman, S. M.; Lin, T. S.; Goldberg, M. P.; Choi, D. W. *J. Neurosci.* **1995**, *15*, 6377–88. Partridge, R. S.; Monroe, S. M.; Parks, J. K.; Johnson, K.; Parker, W. D., Jr.; Eaton, G. R.; Eaton, S. S. *Arch. Biochem. Biophys.* **1994**, *310*, 210–17. Nohl, H.; Jordan, W.; Hegner, D. *FEBS Lett.* **1981**, *123*, 241–4.
- (11) Liu, K.; Sun, J.; Song, Y.-G.; Liu, B.; Xu, Y.-K.; Zhang, S.-X.; Tian, Q.; Liu, Y. *Photosynth. Res.* **2004**, *81*, 41–47. Pospisil, P.; Arato, A.; Krieger-Liszky, A.; Rutherford, A. W. *Biochemistry* **2004**, *43*, 6783–6792. Rahimpour, S.; Palivan, C.; Barbosa, F.; Bilkis, I.; Koch, Y.; Weiner, L.; Fridkin, M.; Mazur, Y.; Gescheidt, G. *J. Am. Chem. Soc.* **2003**, *125*, 1376–1384.
- (12) Xia, Y.; Dawson, V. L.; Dawson, T. M.; Snyder, S. H.; Zweier, J. L. *Proc. Natl. Acad. Sci. U.S.A.* **1996**, *93*, 6770–4. Xia, Y.; Roman, L. J.; Masters, B. S.; Zweier, J. L. *J. Biol. Chem.* **1998**, *273*, 22635–9. Xia, Y.; Tsai, A. L.; Berka, V.; Zweier, J. L. *J. Biol. Chem.* **1998**, *273*, 25804–8.
- (13) Serrano, C. V., Jr.; Mikhail, E. A.; Wang, P.; Noble, B.; Kuppusamy, P.; Zweier, J. L. *Biochim. Biophys. Acta* **1996**, *1316*, 191–202. Varadharaj, S.; Watkins, T.; Cardounel, A. J.; Garcia, J. G. N.; Zweier, J. L.; Kuppusamy, P.; Natarajan, V.; Parinandi, N. L. *Antioxid. Redox Signaling* **2005**, *7*, 287–300.
- (14) Jackson, H. L.; Cardounel, A. J.; Zweier, J. L.; Lockwood, S. F. *Bioorg. Med. Chem. Lett.* **2004**, *14*, 3985–3991. Sankarapandi, S.; Zweier, J. L.; Mukherjee, G.; Quinn, M. T.; Huso, D. L. *Arch. Biochem. Biophys.* **1998**, *353*, 312–321.

While the detection of O₂^{•-} in living cells and *in vivo* tissues has been reported using fluorescence, spectrophotometric, HPLC, and EPR redox probes,²¹ these techniques do not precisely or specifically identify radical production. One of the challenges in biomedical research is to characterize the specific molecular and cellular pathways involved in diseases and to develop genetic, molecular, and pharmacological approaches to prevent or ameliorate free-radical-mediated diseases. In doing so, there is a need for techniques that can unambiguously determine the presence, if not identify the nature, of these reactive species as well as the capability to quantify, to detect *in vivo*, and to locate the site of radical generation in biological systems. The impact of spin-trapping technology on biomedical research can significantly contribute to our understanding of the origin of radical production *in vivo*, the toxicology of xenobiotics, the mechanism of antioxidant activity, the diagnosis of the types of radical damage, and thereby to the development of potential therapeutic properties of spin traps.^{2,4,8,22}

A number of spin traps have been synthesized over the past 10 years with structural motifs different from those of the DMPO-type nitrones, e.g., imidazole,²³ isoindole,²⁴ and indole-one²⁵ nitrones, but these compounds do not effectively trap O₂^{•-}. In the case of trifluoromethyl-pyrroline,²⁶ isoquinoline, and benzazepine²⁷ nitrones, the resulting O₂^{•-} adducts have short half-lives. Moreover, spin adducts of bicyclic nitrones exhibit very complex spectra.²⁸ Although the possibility of designing new nitrones seems endless, there are hurdles typically encountered in the application of new nitrones *in vivo*. To date, only DMPO-substituted nitrones exhibit the most promising spin-trapping properties compared to other nitronone-based spin traps due to their low cytotoxicity²⁹ and their ability to give “finger-

- (15) Wang, P.; Chen, H.; Qin, H.; Sankarapandi, S.; Becher, M. W.; Wong, P. C.; Zweier, J. L. *Proc. Natl. Acad. Sci. U.S.A.* **1998**, *95*, 4556–60. Zweier, J. L.; Flaherty, J. T.; Weisfeldt, M. L. *Proc. Natl. Acad. U.S.A.* **1987**, *84*, 1404. Zweier, J. L.; Kuppusamy, P.; Lutty, G. A. *Proc. Natl. Acad. U.S.A.* **1988**, *85*, 4046. Zweier, J. L.; Kuppusamy, P.; Williams, R.; Rayburn, B. K.; Smith, D.; Weisfeldt, M. L.; Flaherty, J. T. *J. Biol. Chem.* **1989**, *264*, 18890.
- (16) Bosnjakovic, A.; Schlick, S. *J. Phys. Chem. B* **2006**, *110*, 10720–10728. Panchenko, A.; Dilger, H.; Kerres, J.; Hein, M.; Ullrich, A.; Kaz, T.; Roduner, E. *Phys. Chem. Chem. Phys.* **2004**, *6*, 2891–2894.
- (17) Yang, J.; Chen, C.; Ji, H.; Ma, W.; Zhao, J. *J. Phys. Chem. B* **2005**, *109*, 21900–21907. Yu, J.; Chen, J.; Li, C.; Wang, X.; Zhang, B.; Ding, H. *J. Phys. Chem. B* **2004**, *108*, 2781–2783.
- (18) Vakrat-Haglilili, Y.; Weiner, L.; Brumfeld, V.; Brandis, A.; Salomon, Y.; McLroy, B.; Wilson, B. C.; Pawlak, A.; Rozanowska, M.; Sarna, T.; Scherz, A. *J. Am. Chem. Soc.* **2005**, *127*, 6487–6497.
- (19) Nam, S.-N.; Han, S.-K.; Kang, J. W.; Choi, H. *Ultrasonics Sonochem.* **2003**, *10*, 39–147.
- (20) Balakirev, M. Y.; Khramtsov, V. V. *J. Org. Chem.* **1996**, *61*, 7263–7269.
- (21) Dikalov, S.; Skatchkov, M.; Bassenge, E. *Biochem. Biophys. Res. Commun.* **1997**, *230*, 54–57. Rizzi, C.; Samouilov, A.; Kutala, V. K.; Parinandi, N. L.; Zweier, J. L.; Kuppusamy, P. *Free Radical Biol. Med.* **2003**, *35*, 1608–1618.
- (22) Halliwell, B.; Whiteman, M. *Brit. J. Pharmacol.* **2004**, *142*, 231–255.
- (23) Klauschenz, E.; Haseloff, R. F.; Volodarskii, L. B.; Blasig, I. E. *Free Radical Res.* **1994**, *20*, 103–111. Dikalova, A. E.; Kadiiska, M. B.; Mason, R. P. *Proc. Natl. Acad. Sci. U.S.A.* **2001**, *98*, 13549–13553.
- (24) Bottle, S. E.; Micallef, A. S. *Org. Biomol. Chem.* **2003**, *1*, 2581–2584. Bottle, S. E.; Hanson, G. R.; Micallef, A. S. *Org. Biomol. Chem.* **2003**, *1*, 2585–2589.
- (25) Rosen, G. M.; Tsai, P.; Barth, E. D.; Dorey, G.; Casara, P.; Spedding, M.; Halpern, H. J. *J. Org. Chem.* **2000**, *65*, 4460–4463.
- (26) Khramtsov, V. V.; Reznikov, V. A.; Berliner, L. J.; Litkin, A. K.; Grigor'ev, I. A.; Clanton, T. L. *Free Radical Biol. Med.* **2001**, *30*, 1099–1107.
- (27) Thomas, A.; Rajappa, S. *Tetrahedron* **1995**, *51*, 10571–80.
- (28) Stolze, K.; Udilova, N.; Nohl, H. *Biol. Chem.* **2002**, *383*, 813–820. Sankuratri, N.; Kotake, Y.; Janzen, E. G. *Free Radical Biol. Med.* **1996**, *21*, 889–894.
- (29) Rohr-Udilova, N.; Stolze, K.; Marian, B.; Nohl, H. *Bioorg. Med. Chem. Lett.* **2006**, *16*, 541–546. Haseloff, R. F.; Mertsch, K.; Rohde, E.; Baeger, I.; Grigor'ev, I. A.; Blasig, I. E. *FEBS Lett.* **1997**, *418*, 73–75. Khan, N.; Wilmut, C. M.; Rosen, G. M.; Demidenko, E.; Sun, J.; Joseph, J.; O'Hara, J.; Kalyanaraman, B.; Swartz, H. M. *Free Radical Biol. Med.* **2003**, *34*, 1473–81.

3printable” EPR spectra upon reaction with radicals, specifically that of O-centered radicals.² The synthesis of DEPMPO³⁰ and EMPO³¹ provided improvement in the efficiency of spin traps in radical trapping as well as aided in the chemical persistence of the spin adducts obtained and the characteristic EPR spectra they exhibit. However, C-5 substituted nitrones (Chart 1) still suffer major drawbacks such as biostability, cellular target delivery, and slow reactivity toward O₂^{•-}, and these limit their application in the detection of O₂^{•-} in biological systems.

So far, most of our theoretical work,^{32–36} and those by others,³⁷ have focused on the prediction of thermodynamic parameters for the spin-trapping or decomposition process. Although thermodynamic data provide insight into the favorability for formation of certain products, they do not provide kinetic information on the mechanism(s) of spin trapping and spin adduct decay. In this study, second-order rate constants (*k*₂) of superoxide (O₂^{•-}) addition to nitrones in solution have been theoretically predicted. The goals of this study are (1) to validate the conflicting rate constants^{30,38–46} reported in the literature for O₂^{•-} reactions with DMPO, EMPO, and DEPMPO; (2) to demonstrate how theoretically predicted rate constants can reproduce these kinetic values; and (3) to develop an innovative experimental technique for kinetic rate constant determination which can be used to assess the efficiency of newly designed nitrones for their use in spin-trapping applications. In this paper, we describe, from computational as well as experimental perspectives, the reactivity of O₂^{•-} toward various spin traps shown in Chart 1.

2. Computational Methods

2.1. General Procedure. Hybrid density functional theory (DFT)⁴⁷ was employed to obtain optimized geometries and vibrational frequen-

cies for all stationary points at the B3LYP/6-31G(d)⁴⁸ and mPW1K/6-31+G(d,p)⁴⁹ levels of theory. The mPW1K method has been shown by Truhlar and co-workers to be very effective for determining transition state (TS) structures and barrier heights for H-atom transfer reactions.⁵⁰ The mPW1K calculations were initiated by requesting iop(5/45=10000428,5/46=05720572,5/47=10001000) in the route section. Single-point energies were obtained at the B3LYP/6-31+G(d,p) level based on the optimized B3LYP/6-31G(d) geometries. The effect of solvation was investigated with the polarizable continuum model (PCM) for water using single-point energy calculations at the B3LYP/6-31+G(d,p) level and with the gas-phase optimized geometries.⁵¹ All calculations were performed using Gaussian 03.⁵²

Stationary points as minima for both the nitrone spin traps and their respective O₂^{•-} adducts were confirmed to have zero imaginary vibrational frequencies as derived from a vibrational frequency analysis at the B3LYP/6-31G(d) or mPW1K/6-31+G(d,p) levels of theory. Scaling factors of 0.9806⁵³ and 0.9515⁴⁹ were used for the zero-point vibrational energy (ZPE) corrections for the B3LYP and mPW1K geometries, respectively. Free energies were obtained from the calculated thermal and entropic corrections at 298 K using the unscaled vibrational frequencies. For the minima, spin contamination for the adduct radicals are negligible, i.e., 0.75 < ⟨S²⟩ < 0.76 (see Tables S5–S13). Spin densities (populations) and charge densities were obtained from a natural population analysis (NPA) approach at the single-point PCM/B3LYP/6-31+G(d,p)/B3LYP/6-31G(d) and PCM/mPW1K/6-31+G(d,p) levels.⁵⁴ For some selective cases, we explored extensions of the 6-31+G(d,p) basis set by carrying out single-point energy calculations for the reactants, transition states, and products with the more flexible 6-311+G(3df,2p) basis set (see Table S4 for representative adducts).

Initial nitrone and spin adduct structures for transition state (TS) searches were chosen based on the most stable conformer/configuration in aqueous solution via PCM single-point energies on the gas-phase geometries. Fully optimized transition-state structures were confirmed to have one imaginary vibrational frequency and, furthermore, shown to be connected to the desired reactant and product by displacement along the normal coordinate (typically 10%) for the imaginary vibrational frequency in the positive and negative directions, followed by careful minimization using opt = calcfc. Hence, each of the final O₂^{•-} adduct structures reported here is the result of complete geometry optimization after displacement of the TS structure along the reaction coordinate.

To theoretically predict the rate constants for these processes, we examined the potential energy surfaces and located maxima, and we have been successful in locating a variety of TSs for such reactions in the recent past.^{32,55} The ⟨S²⟩ values for the TS have typically shown minimal spin contamination, i.e., 0.76 < ⟨S²⟩ < 0.82. Conventional transition state theory (TST) was utilized to estimate the spin-adduct formation at 298 K.⁵⁶ The conventional TST rate equation in the thermodynamic formulation as a function of temperature is as follows:

$$k(T)_{\text{TST}} = \Gamma(T) \frac{k_{\text{B}}T}{h} \exp(-\Delta G_0^\ddagger/k_{\text{B}}T) \quad (1)$$

In eq 1, *T* is the absolute temperature, *h* is Planck’s constant, *k_B* is Boltzmann’s constant, and Δ*G*₀[‡] is the free energy barrier height

- (30) Frejaville, C.; Karoui, H.; Tuccio, B.; Le Moigne, F.; Culcasi, M.; Pietri, S.; Lauricella, R.; Tordo, P. *J. Med. Chem.* **1995**, *38*, 258–265.
- (31) Olive, G.; Mercier, A.; Le Moigne, F.; Rockenbauer, A.; Tordo, P. *Free Radical Biol. Med.* **2000**, *28*, 403–408.
- (32) Villamena, F. A.; Hadad, C. M.; Zweier, J. L. *J. Phys. Chem. A* **2005**, *109*, 1662–1674.
- (33) Villamena, F. A.; Hadad, C. M.; Zweier, J. L. *J. Phys. Chem. A* **2003**, *107*, 4407–4414. Villamena, F. A.; Hadad, C. M.; Zweier, J. L. *J. Am. Chem. Soc.* **2004**, *126*, 1816–1829.
- (34) Villamena, F. A.; Rockenbauer, A.; Gallucci, J.; Velayutham, M.; Hadad, C. M.; Zweier, J. L. *J. Org. Chem.* **2004**, *69*, 7994–8004.
- (35) Braieda, B.; Hiberty, P. C. *J. Phys. Chem. A* **2000**, *104*, 4618–4628. Locigno, E. J.; Zweier, J. L.; Villamena, F. A. *Org. Biomol. Chem.* **2005**, *3*, 3220–3227. Villamena, F. A.; Merle, J. K.; Hadad, C. M.; Zweier, J. L. *J. Phys. Chem. A* **2005**, *109*, 6089–6098.
- (36) Villamena, F. A.; Merle, J. K.; Hadad, C. M.; Zweier, J. L. *J. Phys. Chem. A* **2005**, *109*, 6083–6088.
- (37) Bentley, J.; Madden, K. P. *J. Am. Chem. Soc.* **1994**, *116*, 11397–11406. Boyd, S. L.; Boyd, R. J. *J. Phys. Chem. A* **2001**, *105*, 7096–7105. Boyd, S. L.; Boyd, R. J. *J. Phys. Chem.* **1994**, *98*, 11705–11713.
- (38) Allouch, A.; Roubaud, V.; Lauricella, R.; Bouteiller, J.-C.; Tuccio, B. *Org. Biomol. Chem.* **2005**, *3*, 2458–2462.
- (39) Finkelstein, E.; Rosen, G. M.; Rauckman, E. J. *J. Am. Chem. Soc.* **1980**, *102*, 4995.
- (40) Frejaville, C.; Karoui, H.; Tuccio, B.; Le Moigne, F.; Culcasi, M.; Pietri, S.; Lauricella, R.; Tordo, P. *J. Chem. Soc., Chem. Commun.* **1994**, 1793–1794.
- (41) Goldstein, S.; Rosen, G. M.; Russo, A.; Samuni, A. *J. Phys. Chem. A* **2004**, *108*, 6679–6685.
- (42) Kezler, A.; Kalyanaraman, B.; Hogg, N. *Free Radical Biol. Med.* **2003**, *35*, 1149–1157.
- (43) Lauricella, R.; Allouch, A.; Roubaud, V.; Bouteiller, J.-C.; Tuccio, B. *Org. Biomol. Chem.* **2004**, *2*, 1304–1309.
- (44) Lauricella, R. P.; Bouteiller, J.-C. H.; Tuccio, B. N. *Phys. Chem. Chem. Phys.* **2005**, *7*, 399–404.
- (45) Tsai, P.; Ichikawa, K.; Mailer, C.; Pou, S.; Halpern, H. J.; Robinson, B. H.; Nielsen, R.; Rosen, G. M. *J. Org. Chem.* **2003**, *68*, 7811–7817.
- (46) Villamena, F. A.; Zweier, J. L. *J. Chem. Soc., Perkin Trans. 2* **2002**, 1340–1344.
- (47) Labanowski, J. W.; Andzelm, J. *Density Functional Methods in Chemistry*; Springer: New York, 1991. Parr, R. G.; Yang, W. *Density Functional Theory in Atoms and Molecules*; Oxford University Press: New York, 1989.
- (48) Becke, A. D. *J. Chem. Phys.* **1993**, *98*, 1372–7. Lee, C.; Yang, W.; Parr, R. G. *Phys. Rev. B* **1988**, *37*, 785–789.
- (49) Lynch, B. J.; Truhlar, D. G. *J. Phys. Chem. A* **2001**, *105*, 2936.
- (50) Lynch, B. J.; Fast, P. L.; Harris, M.; Truhlar, D. G. *J. Phys. Chem. A* **2000**, *104*, 4811.
- (51) Tomasi, J.; Persico, M. *Chem. Rev.* **1994**, *94*, 2027. Cossi, M.; Barone, V.; Cammi, R.; Tomasi, J. *Chem. Phys. Lett.* **1996**, *255*, 327. Barone, V.; Cossi, M.; Tomasi, J. *J. Chem. Phys.* **1997**, *107*, 3210. Barone, V.; Cossi, M.; Tomasi, J. *J. Comput. Chem.* **1998**, *19*, 404. Cossi, M.; Barone, V. *J. Chem. Phys.* **1998**, *109*, 6246.
- (52) Frisch, M. J., et al. *Gaussian 03*, revision B.04 ed.; Gaussian, Inc.: Pittsburgh, PA, 2003.
- (53) Scott, A. P.; Radom, L. *J. Phys. Chem.* **1996**, *100*, 16502–16513.
- (54) Reed, A. E.; Weinhold, F. A.; Curtiss, L. A. *Chem. Rev.* **1998**, *98*, 899.

relative to reactants at infinite separation. The temperature-dependent factor $\Gamma(T)$ represents quantum mechanical tunneling and is accounted for by the Wigner approximation:⁵⁷

$$\Gamma(T) = 1 + \left(\frac{1}{24}\right) \left[1.44 \frac{\nu_i}{T}\right]^2 \quad (2)$$

where ν_i is the imaginary vibrational frequency representing the TS barrier's curvature. Due to spin-orbit coupling in the ${}^2\Pi$ $O_2^{\bullet-}$, population of the first low-lying electronic state was accounted for in the calculation of its electronic partition function. An energy splitting of 160 cm^{-1} , obtained by Parlant and Fiquet-Fayard,⁵⁸ with the ground and excited states both having a degeneracy of 2, was used. Pyrroline *N*-oxides with two equivalent 5-position substituents (i.e., DMPO) have TS structures that are enantiomeric. The rates for reactions with enantiomeric transition states are multiplied by 2 in order to account for the reaction's degeneracy. (While we anticipate that the tunneling correction would be small for a superoxide addition process, we have included this tunneling correction so as to balance the evaluation of possible radical addition and H-atom abstraction reactions.)

2.2. Stopped-Flow Kinetic Experiments. Potassium superoxide (KO_2), phenol red, DMPO, DEPMPO, and 1-methyl-1-carbamoyl-cyclopentane (MCCP) were obtained commercially and used without further purification. 5-Carbamoyl-5-methyl-pyrroline *N*-oxide (AMPO)³⁴ and EMPO³¹ (Chart 1) were synthesized according to the methods previously described. Dry *N,N*-dimethylformamide (DMF) was used at analytical grade (99.9%). Although it has been shown that KO_2 is relatively stable in DMF and dimethylsulfoxide (DMSO) as compared to water,⁵⁹ DMF was chosen over DMSO due to its lower viscosity and since phase partitioning between DMSO and water was observed after mixing in the stopped-flow cell.

Two sets of solutions were prepared for the kinetic measurements. Solution A was freshly prepared by mixing ~200 mg of KO_2 in 5 mL of DMF. The undissolved KO_2 was allowed to settle, and a 1 mL aliquot of the supernatant was obtained and diluted to 10 mL with dry DMF; the tightly covered solution was kept in ice during the course of the experiment. The concentration of $O_2^{\bullet-}$ was quantified and was found to be 10–15 μM based on the absorbance of the peak at 575 nm formed from reaction with phenol red with $O_2^{\bullet-}$ (see below). This concentration remained constant over a period of 35 min (see Figure S2 of the Supporting Information) establishing the stability of KO_2 in DMF during the course of experimentation. Solution B contains varying concentrations of the nitrone spin trap with 500 μM phenol red in 90% DMF–10% water solution.

Stopped-flow reactions were initiated by mixing 150 μL of Solution A with 150 μL of Solution B at room temperature, resulting in final concentrations of phenol red and the spin trap being more than 10 times larger than $[O_2^{\bullet-}]$. The reaction of different spin traps with KO_2 in 95% DMF–5% water solution were followed by the growth of transient absorption at 575 nm ($\epsilon = 7.5 \times 10^4 M^{-1} cm^{-1}$) using a Varian Cary 50 Bio UV–vis spectrophotometer with a stopped-flow accessory. By varying different concentrations of the spin trap of interest, different kinetic curves were obtained at constant concentration of phenol red and $O_2^{\bullet-}$. Kinetic data were fitted to a single-exponential equation.

2.3. Competitive Kinetics. The detailed procedure for EPR spectroscopic investigations is discussed in the Supporting Information and as described in several works by Tuccio and co-workers.^{38,43}

3. Results and Discussion

3.1. Electronic and Structural Properties. 3.1.1. Nitrones.

The selected bond distances based on the optimized geometries at the B3LYP/6-31G(d) level of theory of the nitrone spin traps and their corresponding $O_2^{\bullet-}$ adducts are shown in Table S1 of the Supporting Information. The bond distances for the C=N bond in the nitrone spin traps, the C–N bond in the spin adducts, and the N–O bond in both the nitrones and nitroxides are in good agreement with reported X-ray crystallographic values for comparable compounds.⁶⁰ Optimized bond distances for selected atom pairs in ethoxyphosphoryl, ethoxycarbonyl, carbamoyl, sulfonyl, and trifluoromethyl groups of the nitrones and their respective spin adducts are in good agreement with the reported experimental X-ray crystallographic bond lengths. Intramolecular H-bonding interactions between the amide-H and the nitronyl-O are observed for DiMAPO, AMPO, EMAPO, and MAMPO (Chart 1) with a N–O...H–N hydrogen-bonding distance that ranges from 1.887 Å to 1.978 Å.

Table 1 shows the NPA charges on the C-2 atom (the site of $O_2^{\bullet-}$ addition) of the nitrones at the single-point PCM/B3LYP/6-31+G(d,p)//B3LYP/6-31G(d) and PCM/mPW1K/6-31+G(d,p) levels. (Note: For subsequent discussion, we will refer to the PCM/B3LYP/6-31+G(d,p)//B3LYP/6-31G(d) results simply as B3LYP and PCM/mPW1K/6-31+G(d,p) as mPW1K, unless otherwise noted). It is interesting to note that all of the nitrones with an *N*-methylcarbamoyl substituent as well as AMPO (*N*-methylamide) exhibited the highest NPA positive charge on the C-2 atom (with the exception of the spirolactam nitrone, TAMPO, Chart 1), while the *N,N*-dimethylcarbamoyl-substituted nitrone, DiMAMPO, gave a significantly lower C-2 charge. The absence of an electron-withdrawing substituent, as in the cases of CPPO and DMPO, results in a smaller charge on the C-2 atom. An excellent correlation between B3LYP and mPW1K for the predicted charge densities on the C-2 atom was obtained as shown in Figure S3 of the Supporting Information.

The presence of intramolecular H-bonding in the nitrones was only observed for AMPO and the (monosubstituted) *N*-methylamide nitrones, MAMPO, EMAPO, and DiMAPO. A short N–H_{amide}...O–N_{nitrone} distance was predicted for AMPO, MAMPO, and EMAPO (1.96–1.98 Å), while DiMAPO exhibits two N–H_{amide}...O–N_{nitrone} hydrogen-bonding interactions with distances of 1.98 and 1.89 Å (Figures 1 and 2).}}}}

3.1.2. Tautomers. Amides can undergo tautomerization of the amido-H in solution to form the imidic acid form⁶¹ (Scheme 1 and Figure 1). The calculated free energy differences ($\Delta G_{(aq)} = G_{amide} - G_{imidic\ acid}$) for the amide–imidic acid forms of AMPO, MAMPO, and DiMAPO at the B3LYP level are –15.0, –15.0, and –16.0 kcal/mol, respectively, which indicate that the equilibrium mixture favors the amide isomer and with a very small ($K \sim 10^{-11}$) equilibrium constant for formation of the imidic acid form at 298 K. In TAMPO, lactam–lactim equilibrium gave $\Delta G_{(aq)} = -23.6$ kcal/mol with $K \sim 10^{-18}$ which indicates that the lactim form is even less favored in solution than the formation of imidic acid form. Therefore, the high C-2 charge densities observed for the amido-nitrones are a contribu-

(55) Barckholtz, C.; Barckholtz, T. A.; Hadad, C. M. *J. Phys. Chem. A* **2001**, *105*, 140–15.

(56) Laidler, K. J. *Chemical Kinetics*; Harper & Row, Publishers, Inc.: New York, 1987.

(57) Wigner, E. P. *Z. Phys. Chem. Abt. B* **1932**, *19*, 203.

(58) Parlant, G.; Fiquet-Fayard, F. *J. Phys. B* **1976**, *9*, 1617.

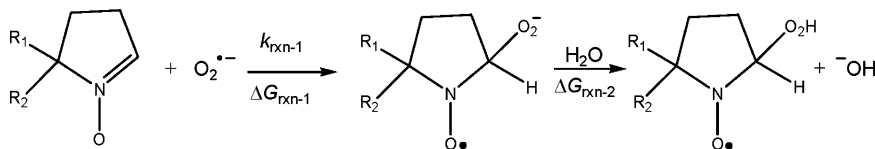
(59) Andrieux, C. P.; Hapiot, P.; Saveant, J.-M. *J. Am. Chem. Soc.* **1987**, *109*, 3768–3775.

(60) Villamena, F.; Dickman, M. H.; Crist, D. R. *Inorg. Chem.* **1998**, *37*, 1446–1453. Boeyens, J. C. A.; Kruger, G. J. *Acta Crystallogr.* **1970**, *B26*, 668. Xu, Y. K.; Chen, Z. W.; Sun, J.; Liu, K.; Chen, W.; Shi, W.; Wang, H. M.; Zhang, X. K.; Liu, Y. *J. Org. Chem.* **2002**, *67*, 7624–7630.

(61) Perrin, C. L.; Lollo, C. P. *J. Am. Chem. Soc.* **1984**, *106*, 2754–7. Wang, W. H.; Hsieh, H. C. *Bull. Chem. Soc. Jpn.* **1994**, *67*, 216–21.

Table 1. Charge Densities of the Nitronyl-C (C-2), and Aqueous Phase Rate Constants (k , $M^{-1} s^{-1}$) and Free Energies of Reaction^a (ΔG_{rxn} , kcal/mol) for the Formation of Superoxide and Hydroperoxyl Adducts at the PCM(water)/mPW1K/6-31+G(d,p) and PCM(water)/B3LYP/6-31+G(d,p)//B3LYP/6-31G(d) Levels of Theory

Energetics of Superoxide Radical Anion Addition to Nitrones



nitrone ^b	PCM/mPW1K/6-31+G(d,p)				PCM/B3LYP/6-31+G(d,p)//B3LYP/6-31G(d)			
	C-2 charge e	k_{rxn1}	ΔG_{rxn1}	ΔG_{rxn2}	C-2 charge e	k_{rxn1}	ΔG_{rxn1}	ΔG_{rxn2}
AMPO	0.054	15.7	1.1	21.2	0.060	38.7	6.1	19.6
DEPMPO	0.038	7.25×10^{-4}	6.4	13.3	0.043	1.50×10^{-5}	14.7	7.3
CPCOMPO	0.040	3.12	5.0	14.3	0.045	6.25×10^{-2}	9.2	13.5
TAMPO	0.034	1.01×10^{-1}	5.7	13.8	0.038	2.69×10^{-3}	9.7	12.8
EMPO	0.035	3.92×10^{-1}	4.9	13.5	0.040	6.77×10^{-2}	9.7	11.5
TFMPO	0.038	14.2	4.4	14.1	0.043	1.32	8.8	12.8
CPPO	0.015	2.48×10^{-2}	5.8	13.6	0.024	4.00×10^{-3}	10.5	12.1
DMPO	0.013	3.16×10^{-3}	8.3	11.3	0.019	5.85×10^{-5}	11.9	10.9
DEPO	0.039	2.09×10^{-1}	3.5	14.3	0.043	2.07×10^{-4}	12.4	8.8
MAMPO	0.056	8.06	2.9	19.9	0.060	2.44×10^{-1}	4.3	22.3
DiMAMPO	0.026	1.62×10^{-2}	6.3	12.7	0.030	1.26×10^{-4}	11.3	11.3
DiMAPO	0.092	3.52×10^{-2}	0.7	21.5	0.098	8.91×10^{-4}	6.2	18.3
EMAPO	0.069	13.0	2.1	20.6	0.073	1.92	8.0	18.4

^a Energetics are derived from the superoxide radical adduct structures resulting from their respective TS structure. ^b See Chart 1 for the structures of the nitrones.

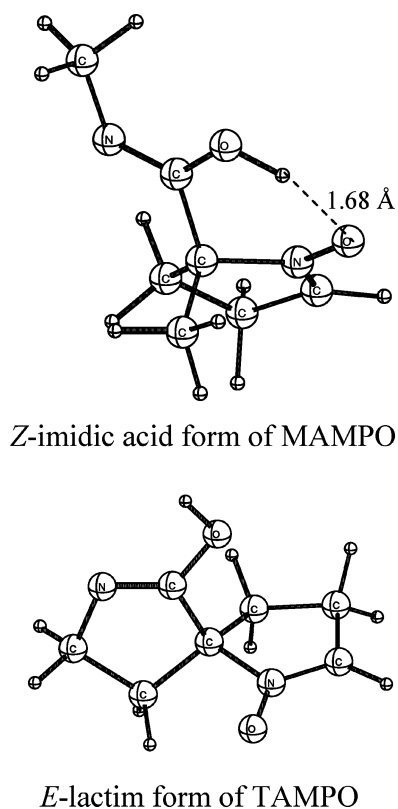


Figure 1. Optimized structures of the most stable *E*-imidic acid and *Z*-lactim forms of MAMPO and TAMPO, respectively, at the B3LYP/6-31G(d) level of theory.

tion from the amido tautomers. Further discussion on the structural and electronic properties of the imidic acid and lactim forms, in comparison to the amide and lactam forms, is presented in the Supporting Information.

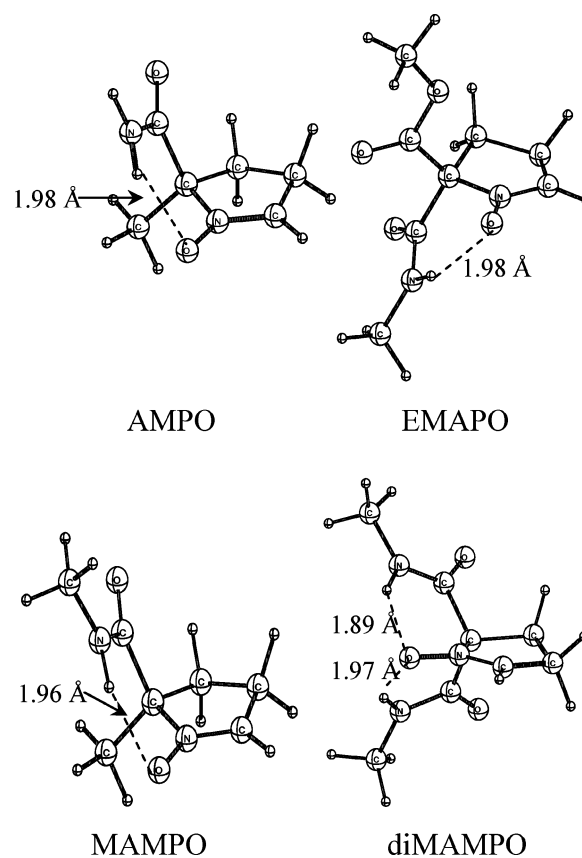
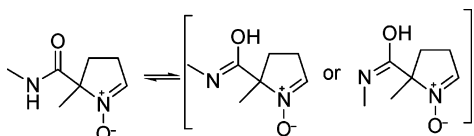
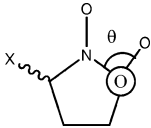


Figure 2. Preferred geometries for the optimized structures of amide-based nitrones at the B3LYP/6-31G(d) level showing strong intramolecular H-bonding interactions.

3.1.3. Superoxide Adducts. The structures of the superoxide spin adducts have O—O bond distances ranging from 1.40 to 1.48 Å in all of the $O_2^{\bullet-}$ adducts. The $C_{ring}-O_2^-$ bond distances

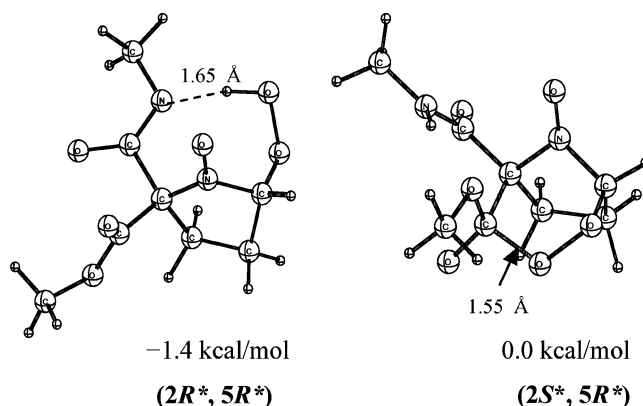
Scheme 1. Tautomerism in Monosubstituted *N*-Methylamide Nitrone, MAMPO**Table 2.** Superoxide Adducts Resulting from Their Respective Transition State Structures at the B3LYP/6-31G(d) and mPW1K/6-31+G(d,p) (in Parentheses) Levels of Theory


O ₂ ^{•-} adducts	θ (deg)
AMPO-cis	48.9 (48.8)
DEPMPO-cis	188.5 (183.7)
CPCOMPO-cis	188.3 (184.4)
TAMPO-cis	187.7 (183.1)
EMPO-trans	193.1 (187.5)
TFMPO-trans	194.0 (189.7)
CPPO	194.6 (186.0)
DMPO	192.4 (290.1)
DEPO	291.4 (290.7)
MAMPO-cis	286.2 (47.7)
DiMAMPO-cis	76.5 (72.2)
DiMAPO	45.7 (45.8)
EMAPO ^a	43.5 (44.4)
MSMPO	n/a

^a Where the -O₂^{•-} group is *cis* to the amide group.

are in the range of 1.37–1.43 Å, similar to that observed experimentally for cyclic hydroperoxides of 1.46 Å.⁶² The final O₂^{•-} adduct structures favor the *cis* configuration (i.e., the superoxide moiety is *cis* to the highest priority ring substituent) with the exception of EMPO and TFMPO in which the *trans* configuration is preferred. An O–O–C–N dihedral angle range of 188.3° to 283.6° was predicted for the O₂^{•-} adducts, except for the O₂^{•-} adducts of the amido-nitrones AMPO, DiMAPO, and EMAPO in which lower O–O–C–N dihedral angles (~45°) were observed at the B3LYP and mPW1K levels (Table 2). These lower O–O–C–N dihedral angles are due to the strong N–H...O–O intramolecular H-bonding interactions providing distances from 1.03 to 1.05 Å. The predicted O–O–C–N dihedral angles at the B3LYP level correlates well with the mPW1K angles, with the exception of MAMPO–O₂^{•-} in which the predicted O–O–C–N dihedral angles were 286.2° and 47.7° at the B3LYP and mPW1K levels, respectively. The high O–O–C–N dihedral angle of 286.2° for MAMPO–O₂^{•-} at the B3LYP result from a weaker N–H...O–O interaction of 1.47 Å compared to 1.06 Å predicted at the mPW1K level. In the case of the DEPO–O₂ adduct, intramolecular nucleophilic addition of the peroxide-O to the carbonyl-C was predicted with an O–O...C=O bond distance of 1.58 Å similar to that predicted for the least preferred isomer *cis*-EMPO–O₂ from our previous work.³²

Figure 3 shows the most favored EMAPO spin adduct isomers, (2*R**,5*R**) and (2*S**,5*R**), in which the amido group is *cis* or *trans* to the O₂^{•-} moiety, respectively. The EMAPO–O₂ isomer that exhibits a strong N–H...O–O interaction is

**Figure 3.** Relative free energies in aqueous phase ($\Delta G_{298K, aq}$ in kcal/mol) of optimized EMAPO–O₂^{•-} adducts showing strong intramolecular interactions at the PCM(water)/B3LYP/6-31+G(d,p)//B3LYP/6-31G(d) level. Note that the preferred isomer is (2*R**,5*R**)-EMAPO–O₂^{•-} in which the superoxide unit is in a *cis* position to the amide group.

predicted to be more favored than the isomer exhibiting an O=C...OO interaction by 1.4 kcal/mol. Spin density (population) distributions in some nitronium–O₂^{•-} adducts have also been discussed in our previous work.³²

3.1.4. Transition State Structures. TS structures for the formation of the O₂^{•-} adducts were calculated, and evaluation of the analytical (harmonic) force constants gave a single negative eigenvalue (hence, one imaginary vibrational frequency) that corresponded to the motion along the C_{nitronyl}–C[–]–O_{superoxide} axis (Table 3). A range of imaginary vibrational frequencies from 311 to 559*i* cm^{–1} and 199–917*i* cm^{–1} were predicted for the various O₂^{•-} addition TSs at the B3LYP and mPW1K levels, respectively.

A wide range of TS [C_{ring}...O₂^{•-}][‡] distances at the B3LYP (1.66 to 2.08 Å) and at the mPW1K (1.61 to 2.06 Å) level were observed. The calculated [C_{ring}...O₂^{•-}][‡] bond distances are intermediate between the C–O bond distances calculated for the formed complexes and the final product (Table 3). Moreover, the average of the sum of the ∠N–C(2)–H, ∠N–C(2)–C(3), and ∠C(3)–C(2)–H angles in all of the TS structures for O₂^{•-} addition at the B3LYP level are intermediate (i.e., 346.2 ± 4.7°) to the sum of the angles predicted for an sp² hybridized C(2) of the nitrones (i.e., 359.8 ± 0.3°) and the respective sp³ hybridized C(2) of the spin adducts (i.e., 326.4 ± 1.8°). On the basis of Hammond's postulate, these results suggest that the TS structures for the O₂^{•-} addition resemble the reactant structures to a greater extent. A discussion on the spin density distribution in the TS structures is presented in the Supporting Information (see p S22).

Monosubstituted *N*-methylamide nitrones exhibited N–H...O–O H-bonding interaction at the TS (see Figure 4). The observed [N–H...O–O][‡] H-bond lengths in the TS structures for O₂^{•-} addition of AMPO and EMAPO are slightly longer by 0.5 Å compared to the N–H...O–O H-bond distances of their respective products (~1.0 Å), while the [N–H...O–O][‡] bond lengths in O₂^{•-} adducts of MAMPO (1.65 Å) and DiMAPO (1.04 Å) did not change in the final product (see Figure S4 of the Supporting Information for the pertinent bond lengths in the O₂^{•-} adduct structures). These predicted intramolecular interactions in the TS can play a role in the stabilization of the TS structures and, hence, in the facile formation of the final products. All of these predicted H-bonding interactions in the

(62) Alini, S.; Citterio, A.; Farina, A.; Fochi, M. C.; Malpezzi, L. *Acta Crystallogr.* **1998**, *C54*, 1000–1003.

Table 3. Calculated Relative Enthalpies ΔH_{298K} and Free Energies ΔG_{298K} (kcal/mol) in Aqueous Phase and Other Theoretical Parameters for the TS Structures of the O₂^{•-} Addition at the PCM/mPW1K/6-31+G(d,p) and PCM/B3LYP/6-31+G(d,p)//B3LYP/6-31G(d) (in Parentheses) Levels of Theory

structure	$\Delta H_{298K, aq}^e$	$\Delta G_{298K, aq}^e$	C---O ₂ ^{•-} Å	$\langle S^2 \rangle$	imaginary frequency ^g
AMPO					
AMPO + O ₂ ^{•-} ^a	0.0 (0.0)	0.0 (0.0)	∞	<i>f</i>	
AMPO --- O ₂ ^{•-} ^b	-1.4 (-0.1)	7.3 (8.6)	4.04 (3.51)	0.76 (0.76)	0
[AMPO-O ₂ ^{•-}] ^{†c}	6.7 (5.7)	17.9 (17.4)	1.90 (1.80)	0.81 (0.78)	511i (545i)
AMPO-O ₂ ^{•-} ^d	-10.6 (-5.5)	1.1 (6.1)	1.41 (1.42)	0.76 (0.75)	0
DEPMPO					
DEPMPO + O ₂ ^{•-}	0.0 (0.0)	0.0 (0.0)	∞	<i>f</i>	
DEPMPO --- O ₂ ^{•-}	2.6 (6.5)	11.1 (16.4)	2.86 (2.53)	0.76 (0.77)	0
[DEPMPO-O ₂ ^{•-}] [†]	12.1 (14.7)	23.7 (26.1)	1.63 (1.66)	0.76 (0.75)	199i (391i)
DEPMPO-O ₂ ^{•-}	-4.5 (3.4)	6.4 (14.7)	1.38 (1.43)	0.76 (0.76)	0
DMPO					
DMPO + O ₂ ^{•-}	0.0 (0.0)	0.0 (0.0)	∞	<i>f</i>	
DMPO --- O ₂ ^{•-}	3.1 (5.3)	10.4 (14.1)	3.07 (2.69)	0.76 (0.76)	0
[DMPO-O ₂ ^{•-}] [†]	13.4 (14.9)	23.4 (25.7)	1.80 (1.81)	0.78 (0.78)	611i (546i)
DMPO-O ₂ ^{•-}	-2.5 (1.0)	8.3 (11.9)	1.37 (1.41)	0.75 (0.75)	0
EMPO					
EMPO + O ₂ ^{•-}	0.0 (0.0)	0.0 (0.0)	∞	<i>f</i>	
EMPO --- O ₂ ^{•-}	2.5 (3.5)	10.2 (12.2)	2.77 (2.71)	0.76 (0.76)	0
[EMPO-O ₂ ^{•-}] [†]	10.1 (11.4)	20.1 (21.1)	1.71 (1.77)	0.76 (0.76)	586i (498i)
EMPO-O ₂ ^{•-}	-5.3 (-0.6)	4.9 (9.7)	1.39 (1.41)	0.76 (0.76)	0
CPCOMPO					
CPCOMPO + O ₂ ^{•-}	0.0 (0.0)	0	∞	<i>f</i>	
CPCOMPO --- O ₂ ^{•-}	2.8 (4.1)	9.7 (12.6)	3.07 (2.63)	0.76 (0.77)	0
[CPCOMPO-O ₂ ^{•-}] [†]	8.5 (11.0)	18.7 (21.2)	1.68 (1.71)	0.76 (0.76)	274i (504i)
CPCOMPO-O ₂ ^{•-}	-5.6 (-1.3)	4.9 (9.2)	1.38 (1.41)	0.76 (0.76)	0
TAMPO					
TAMPO + O ₂ ^{•-}	0.0 (0.0)	0.0 (0.0)	∞	<i>f</i>	
TAMPO --- O ₂ ^{•-}	3.1 (4.5)	9.9 (12.7)	3.29 (2.74)	0.76 (0.76)	0
[TAMPO-O ₂ ^{•-}] [†]	10.8 (12.9)	20.8 (23.0)	1.67 (1.72)	0.76 (0.76)	333i (529i)
TAMPO-O ₂ ^{•-}	-4.9 (-0.7)	5.6 (9.7)	1.38 (1.41)	0.76 (0.76)	0
TFMPO					
TFMPO + O ₂ ^{•-}	0.0 (0.0)	0.0 (0.0)	∞	<i>f</i>	
TFMPO --- O ₂ ^{•-}	2.5 (3.7)	10.4 (11.7)	2.69 (2.61)	0.76 (0.76)	0
[TFMPO-O ₂ ^{•-}] [†]	8.0 (9.7)	18.0 (19.3)	1.72 (1.80)	0.76 (0.75)	536i (374i)
TFMPO-O ₂ ^{•-}	-6.0 (-1.7)	4.4 (8.8)	1.39 (1.42)	0.76 (0.76)	0
DEPO					
DEPO + O ₂ ^{•-}	0.0 (0.0)	0.0 (0.0)	∞	<i>f</i>	
DEPO --- O ₂ ^{•-}	3.3 (5.1)	12.7 (15.9)	2.87 (2.77)	0.76 (0.76)	0
[DEPO-O ₂ ^{•-}] [†]	10.8 (14.4)	21.1 (25.0)	1.61 (1.80)	0.76 (0.77)	917i (559i)
DEPO-O ₂ ^{•-}	-9.4 (-1.0)	3.4 (12.4)	1.40 (1.40)	0.76 (0.75)	0
CPPO					
CPPO + O ₂ ^{•-}	0.0 (0.0)	0.0 (0.0)	∞	<i>f</i>	
CPPO --- O ₂ ^{•-}	3.4 (4.8)	10.8 (13.9)	2.91 (2.67)	0.76 (0.76)	0
[CPPO-O ₂ ^{•-}] [†]	12.1 (12.9)	22.2 (23.2)	1.72 (1.75)	0.76 (0.76)	639i (542i)
CPPO-O ₂ ^{•-}	-4.1 (0.7)	5.8 (10.5)	1.39 (1.41)	0.76 (0.76)	0
MAMPO					
MAMPO + O ₂ ^{•-}	0.0 (0.0)	0.0 (0.0)	∞	<i>f</i>	
MAMPO --- O ₂ ^{•-}	-1.9 (0.8)	7.1 (10.5)	4.00 (2.88)	0.76 (0.76)	0
[MAMPO-O ₂ ^{•-}] [†]	6.4 (9.2)	18.0 (20.3)	1.90 (2.01)	0.80 (0.79)	513i (343i)
MAMPO-O ₂ ^{•-}	-9.3 (-7.6)	2.8 (4.3)	1.41 (1.38)	0.76 (0.75)	0
DiMAMPO					
DiMAMPO + O ₂ ^{•-}	0.0 (0.0)	0.0 (0.0)	∞	<i>f</i>	
DiMAMPO --- O ₂ ^{•-}	3.0 (4.6)	12.5 (14.7)	2.68 (2.63)	0.76 (0.76)	0
[DiMAMPO-O ₂ ^{•-}] [†]	10.4 (13.0)	21.9 (24.8)	1.66 (1.70)	0.76 (0.75)	265i (311i)
DiMAMPO-O ₂ ^{•-}	-5.6 (-0.6)	6.3 (11.3)	1.37 (1.39)	0.76 (0.76)	0
EMAPO					
EMAPO + O ₂ ^{•-}	0.0 (0.0)	0.0 (0.0)	∞	<i>f</i>	
EMAPO --- O ₂ ^{•-}	-2.4 (-0.9)	6.7 (8.6)	4.02 (3.97)	0.76 (0.76)	0
[EMAPO-O ₂ ^{•-}] [†]	6.2 (7.4)	18.0 (19.1)	1.92 (1.93)	0.81 (0.80)	516i (472i)
EMAPO-O ₂ ^{•-}	-9.9 (-4.2)	2.1 (8.0)	1.42 (1.43)	0.75 (0.75)	0
DiMAPO					
DiMAPO + O ₂ ^{•-}	0.0 (0.0)	0.0 (0.0)	∞	<i>f</i>	
DiMAPO --- O ₂ ^{•-}	-3.2 (-1.2)	7.8 (8.7)	4.03 (4.00)	0.76 (0.75)	0
[DiMAPO-O ₂ ^{•-}] [†]	8.2 (11.7)	21.9 (24.0)	2.06 (2.08)	0.82 (0.81)	450i (411i)
DiMAPO-O ₂ ^{•-}	-13.2 (-6.5)	0.7 (6.2)	1.42 (1.43)	0.75 (0.75)	0

^a At infinite separation. ^b Nitron --- O₂^{•-} complex. ^c Transition state. ^d Products. ^e Values are relative energies based on single-point energy calculations with the polarizable continuum model (PCM) at the mPW1K/6-31+G(d,p) level using water as a solvent. Values in parentheses are at the PCM/B3LYP/6-31+G(d,p)//B3LYP/6-31G(d) level. Thermal and entropic corrections from the gas-phase calculations were applied with the single-point energy for the PCM level in order to get an estimated ΔH_{298K} and ΔG_{298K} in water. ^f The $\langle S^2 \rangle$ for all the nitrones is 0.00, while that of O₂^{•-} is 0.75–0.76 at both levels of theory used. ^g Point group for all structures is C₁, and imaginary vibrational frequencies are in the units of cm⁻¹.

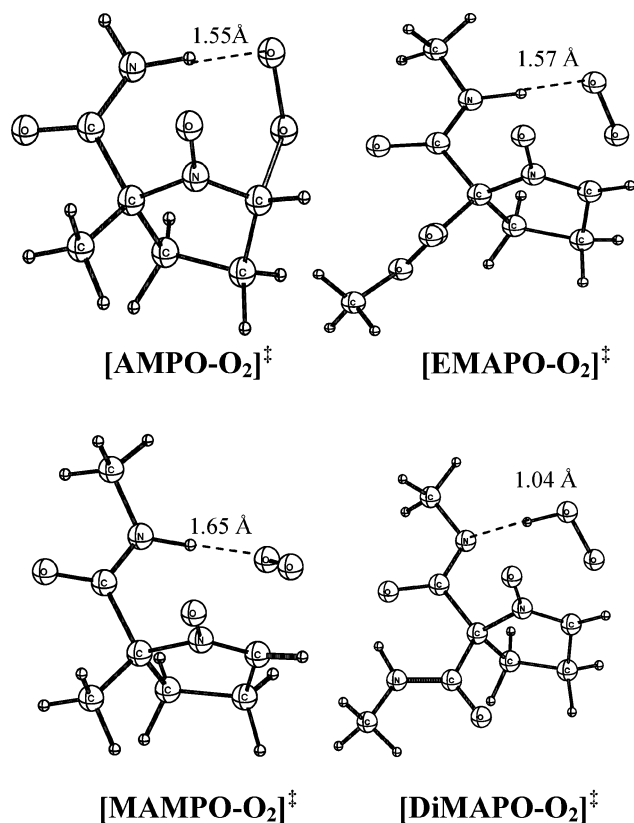


Figure 4. Transition state structures for formation of $O_2^{\bullet-}$ adducts of monosubstituted *N*-alkylamide nitrones showing the early formation of an intramolecular H-bonding interaction between the amide and superoxy groups at the B3LYP/6-31G(d) level. A complete diagram of the TS structures can be found in the Supporting Information.

transition states have been observed at both B3LYP/6-31G(d) and mPW1K levels of theory.

3.1.5. Calculated Isotropic Hyperfine Splitting Constants.

In order to justify the DFT approach employed in this study, the electron spin distribution within the nitron– O_2H adducts was assessed from the calculated isotropic hyperfine splitting constant (hfsc), $a_{(X)}$. The calculated hfsc's in the gas phase at the B3LYP level for the four model adducts, i.e., AMPO– O_2H , DMPO– O_2H , EMPO– O_2H and DEPMPO– O_2H , were previously obtained (see p S39 of the Supporting Information of our previous paper³⁴), and the Boltzmann-weighted hfsc's of the various conformers were compared with their respective experimental hfsc's (Figure S1) in aqueous and DMSO solutions as shown in Table S2. The data show reasonable agreement between the theoretical and experimental data further validating the DFT approach employed in this study. The relationship between the calculated and experimental hfsc's are further discussed in the Supporting Information (see p S6).

3.2. Determination of Theoretical Rate Constants.

3.2.1. General. Table 1 shows the calculated charge densities on the nitronyl-C as well as the aqueous-phase rate constants and free energies of reaction for the formation of nitron– O_2H adducts via direct addition of $O_2^{\bullet-}$ to the various nitrones, followed by a proton transfer at the B3LYP and mPW1K levels of theory. In our earlier studies,^{34,36} we showed that there are two possible mechanisms for the formation of DMPO– O_2H in aqueous solution. At neutral (and higher) pH, the addition of $O_2^{\bullet-}$ to DMPO can lead to the formation of the DMPO– $O_2^{\bullet-}$ adduct, followed by subsequent protonation to form the final

DMPO– O_2H spin adduct. In acidic medium, DMPO– O_2H can be formed via direct addition of HO_2^{\bullet} from the protonated $O_2^{\bullet-}$. Experimental kinetic data support these two mechanisms based on the strong pH dependence of the rate of $O_2^{\bullet-}$ trapping. The higher second-order rate constants^{39,45} observed at lower pH is due to the higher concentration of the more reactive HO_2^{\bullet} in more acidic media. Hence, to narrow down the scope of this work, we will only present the energetics of $O_2^{\bullet-}$ addition to nitrones. The energetics of HO_2^{\bullet} trapping by the same family of nitrones will be presented in a separate work in which the predicted k and ΔG_{rxn} were found to be in the range of 10^1 to 10^3 $M^{-1} s^{-1}$ and -5 to -11 kcal/mol, respectively, and are consistent with available experimental observations.^{39,45}

3.2.2. Correlation of Calculated Charge Densities, Free Energies, and Rate Constants. Figure 5a shows the relationship between the charge densities on the nitronyl-C (C-2) of various nitrones with the free energies of reaction (ΔG_{rxn-1} , Table 1) for $O_2^{\bullet-}$ addition to nitrones at the mPW1K level; the resulting plot has a reasonable correlation ($r^2 = 0.78$). Indeed, Figure 5a demonstrates that the free energy (ΔG_{rxn-1}) for $O_2^{\bullet-}$ addition to nitrones increases with an increasing positive charge on C-2 of the nitrones. Also, a general trend of increasing reaction rate for $O_2^{\bullet-}$ addition to these nitrones ($\log k_{rxn-1}$) with increasing C-2 charge of the nitron can be seen in Figure 5b with $r^2 = 0.76$ (excluding DEPMPO and DiMAPO as outliers). The same qualitative trend was observed at the B3LYP level of theory (Figure S5a,b, Supporting Information) but with a smaller correlation of $r^2 = 0.48$ compared to the mPW1K level. Figure 5c (and Supporting Information, Figure S5c) shows the cross correlation between the thermodynamic entities ΔG_{rxn-1} and $\log k_{rxn-1}$ using and B3LYP levels with reasonable correlation values of $r^2 = 0.73$ and 0.89 , respectively. Figure S6 shows a large correlation between the B3LYP and mPW1K levels for the ΔG_{rxn} and $\log k_{rxn-1}$ of $O_2^{\bullet-}$ addition to nitrones in aqueous phase at 298 K with $r^2 = 0.55$ and 0.87 , respectively.

From our previous study,⁴⁶ we postulated (in analogy to Hammond's postulate as well as the Bell–Evans–Polanyi principle)⁶³ that the rate of $O_2^{\bullet-}$ addition to nitrones can be correlated with the free energy of reaction (ΔG_{rxn-1}). Since ΔG is a thermodynamic entity, it is not so convincing to assume that this trend could be used to explain the differences in experimental rate constants observed for the addition of $O_2^{\bullet-}$ to various nitrones. The theoretical correlation between $\log k_{rxn-1}$ and the C-2 charge densities of the nitrones is quite good and is similar to that for the free energy of reaction in these systems, thereby confirming our earlier assumption^{32,46} as to the direct relationship between the free energy of reaction and the rate of $O_2^{\bullet-}$ addition to nitrones.

3.2.3. Superoxide Radical Anion Reactivity. To obtain more insight into the observed reactivity of $O_2^{\bullet-}$ and its nucleophilic character, there is a need to compare its reactivity against that of other radicals. On the basis of purely thermodynamic considerations, our previous studies^{32,33,46} showed that the order of increasing thermodynamic favor ($\Delta G_{rxn,aq,298K}$ (kcal/mol)) for the addition of different radicals to various nitrones using a PCM model for water is as follows: NO (14.1) < $O_2^{\bullet-}$ (10.0) < HO_2^{\bullet} (–7.0) < HS^{\bullet} (–13.6) < $\bullet CH_3$ (–32.9) < HO^{\bullet} (–38.9). The σ -type radicals (HS^{\bullet} , $\bullet CH_3$, and HO^{\bullet}) have exhibited higher

(63) Evans, M. G.; Polanyi, M. *Trans. Faraday Soc.* **1936**, *32*, 1333–60. Evans, M. G.; Polanyi, M. *Trans. Faraday Soc.* **1938**, *34*, 11–24.

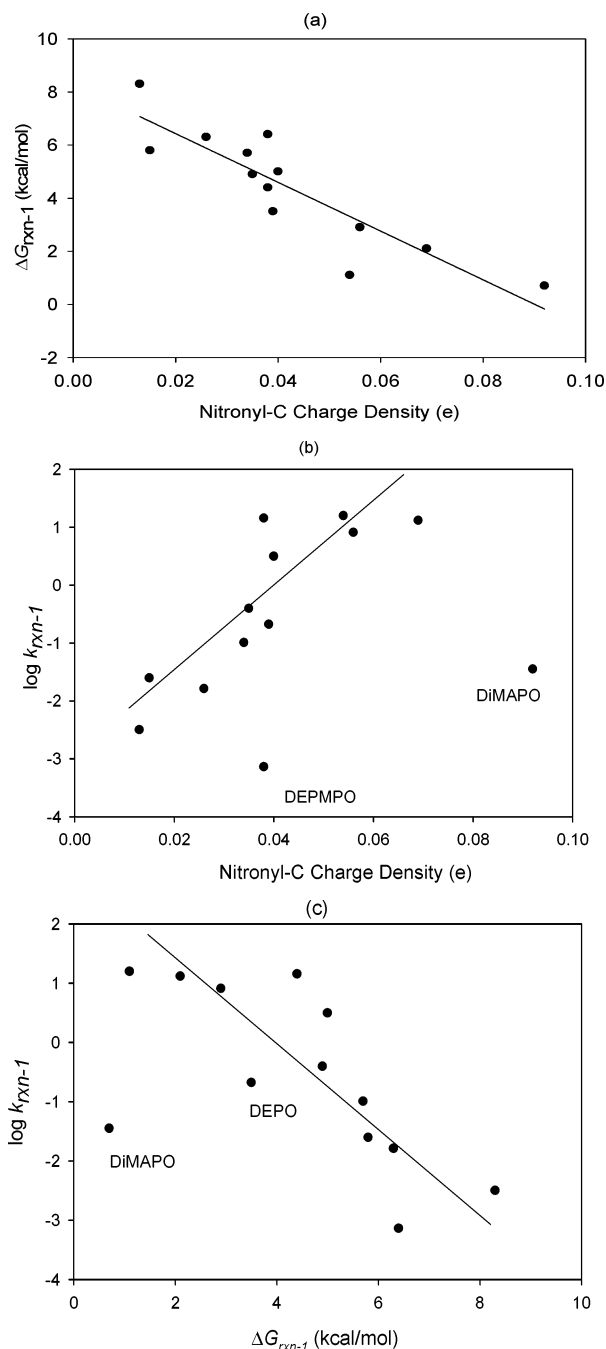


Figure 5. Correlation of the nitronyl-C (C-2) charge densities with (a) free energies ($\Delta G_{\text{rxn}-1, 298\text{K}}$, kcal/mol) ($r^2 = 0.78$) and (b) rate constants ($\log k_{\text{rxn}-1}$) of $O_2^{\bullet-}$ addition to nitrones in the aqueous phase at the PCM(water)/mPW1K/6-31+G(d,p) level of theory at 298 K ($r^2 = 0.76$, excluding the outliers DEPMPPO and DIMAPO). (c) Degree of correlation between $\log k_{\text{rxn}-1}$ and $\Delta G_{\text{rxn}-1}$ at the same level of theory with $r^2 = 0.73$ excluding the outliers (DIMAPO and DEPO).

reactivity compared to the π -type radicals, NO, $O_2^{\bullet-}$, and HO_2^{\bullet} . In general, this trend in reactivity follows the order of the degree of spin density residing on the attacking atom of the radical, i.e., 100% spin density on the O, S, and C atoms of HS^{\bullet} , $\bullet CH_3$, and HO^{\bullet} , compared to 70% (N), 50% (O), and 73% (terminal O) spin density distribution in NO, $O_2^{\bullet-}$, and HO_2^{\bullet} , respectively. The HO^{\bullet} addition to electron-rich double bonds is commonly considered to be electrophilic in nature and possesses some electron-transfer character from the electron-rich substrate to the HO^{\bullet} radical.^{64,65} Our thermodynamic results^{32,33} also show

that the exoergicity of the HO^{\bullet} addition to electron-poor nitrones increases with the increasing positive charge on the (C-2) nitronyl-C which suggests that the reaction of HO^{\bullet} addition to nitrones is partly nucleophilic in character. The same partial electrostatic effect on radical reactivity was also observed for the π -type radicals, such as NO, $O_2^{\bullet-}$, and HO_2^{\bullet} , for which there is a significant difference in the charge densities of the attacking atom, i.e., +0.20 e, -0.50 e, and -0.15 e, respectively, in spite of the similarities, for example, in the spin density distribution on the N and O atoms of the NO and HO_2^{\bullet} , respectively. However, unlike $O_2^{\bullet-}$, the dependence of radical-addition reactivity for all of these radicals to add to nitrones is not significantly pronounced for the varying charge density on the nitronyl-C.³² This result is probably due to the considerable (high) spin density distribution on the attacking atoms (70%–100%); hence, the electrophilicity of the radicals dominates.

Moreover, the relative thermodynamic favorability of radical addition toward nitrones is consistent with the reported reduction potentials (hence, their electron affinities, EA) for these various radicals.^{32,66} The low electron affinity of $O_2^{\bullet-}$ can contribute significantly toward a high activation barrier and a slower rate constant of adduct formation. All of the other radicals have more favorable EA values and can undergo facile reduction with the exception of NO in which the formation of triplet NO^- is not favored. Based on these predictions, it can be inferred that for $O_2^{\bullet-}$, given the high negative charge density and low spin density distribution on the attacking atom, the nature of radical addition to nitrones is mostly nucleophilic. These factors are consistent with the earlier suggestions for HO^{\bullet} addition to aromatic hydrocarbons.^{65,67}

3.2.4. Nitronyl Reactivity. As shown in Table 1, the theoretically predicted rate constants in the aqueous (PCM) phase for $O_2^{\bullet-}$ addition to nitrones range from 7.25×10^{-4} to $15.7 \text{ M}^{-1} \text{ s}^{-1}$ with the formation of $O_2^{\bullet-}$ adducts from the monosubstituted *N*-methylamide nitrones (AMPO, MAMPO, and EMAPO), and that of TFMPO are the most kinetically favored at the mPW1K level, while DEPMPPO gave the slowest rate constant, followed by DMPO, DiMAMPO, and CPPO. Even *trans* $O_2^{\bullet-}$ addition to DEPMPPO only gave a $k_{\text{rxn}-1}$ of $5.48 \times 10^{-2} \text{ M}^{-1} \text{ s}^{-1}$ (see Table S15 and S16). Intermediate rate constants were predicted for the alkoxy carbonyl substituted nitrones, CPCOMPO, EMPO, and DEPO, and the amide, TAMPO. The same qualitative trend has been observed at the B3LYP level with AMPO, MAMPO, EMAPO, and TFMPO yielding the highest rate constants (Table 1). The ease of formation of $O_2^{\bullet-}$ adducts in monosubstituted *N*-monoalkylamide nitrones is due to the relatively high positive charge on the C-2 position as well as the early formation of H-bonding interaction between the amide-H and the $O_2^{\bullet-}$ (as shown in Figure 4), thereby facilitating the formation of the $O_2^{\bullet-}$ adduct. These data suggest that the use of 5,5-disubstituted nitrones with electron-withdrawing alkoxy carbonyl and monoalkylcarbamoyl substituents could be ideal multifunctional spin

(64) von Sonntag, C. *The Chemical Basis of Radiation Biology*; Taylor and Francis: New York, 1987. Imamura, A.; Hirao, K. *Bull. Chem. Soc. Jpn.* **1979**, *52*, 287–92.

(65) DeMatteo, M. P.; Poole, J. S.; Shi, X.; Sachdeva, R.; Hatcher, P. G.; Hadad, C. M.; Platz, M. S. *J. Am. Chem. Soc.* **2005**, *127*, 7094–7109.

(66) Bartberger, M. D.; Liu, W.; Ford, E.; Miranda, K. M.; Switzer, C.; Fukuto, J. M.; Farmer, P. J.; Wink, D. A.; Houk, K. N. *Proc. Natl. Acad. Sci. U.S.A.* **2002**, *99*, 10958–10963. Buettner, G. R. *Arch. Biochem. Biophys.* **1993**, *300*, 535–543. Das, T. N.; Huie, R. E.; Neta, P.; Padmaja, S. A. *J. Phys. Chem. A* **1999**, *103*, 5221–5226.

(67) Poole, J. S.; Shi, X.; Hadad, C. M.; Platz, M. S. *J. Phys. Chem. A* **2005**, *109*, 2547–2551.

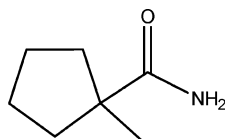
Table 4. Polarizable Continuum Model (PCM) Calculation of Fully Optimized Structure at the PCM/B3LYP/6-31+G(d,p) Level of Theory at 298 K

spin trap (ST)	charge density (C-2) ^a	[ST-O ₂ ^{•-}] ^b		<i>k</i> ₂ (M ⁻¹ s ⁻¹)
		Δ <i>H</i> [‡]	Δ <i>G</i> [‡]	
AMPO	0.035	8.1	19.4	1.24
DMPO	-0.001	12.8	22.6	1.29 × 10 ⁻²

^a Calculated C-2 charge densities for DEPMPO and EMPO are 0.022 and 0.015 e, respectively. ^b Relative to energies at infinite separation.

traps in which target-specific and adduct-stabilizing moieties can be tethered in the parent nitron molecule employing ester or amide units as linker groups.

3.2.5. Effect of the Amide Moiety on Thermodynamics of O₂^{•-} Addition. The contribution of H-bonding interactions on the reaction energies, however, remains ambiguous; therefore 1-methyl-1-carbamoylcyclopentane (MCCP) was used to investigate the nonelectrostatic contribution to the free energies of reaction with O₂^{•-}. The use of MCCP is ideal since it carries



1-methyl-1-carbamoylcyclopentane (MCCP)

almost all of the structural features of AMPO but without the nitron moiety and, therefore, only considers the reaction energy contribution from the amide-H interaction with O₂^{•-}. Results show that, at the mPW1K level, the Δ*G*_{rxn,298K} for the complex formation due to the N-H...O₂^{•-} interaction from MCCP is 6.4 kcal/mol endoergic which is close to the value of 7.6 kcal/mol predicted for AMPO at the same level of theory. Moreover, the calculated free energies of reaction for O₂^{•-} addition to AMPO in the absence of intramolecular H-bonding interaction for both *cis* and *trans* isomers at the mPW1K level are Δ*G*_{rxn,298K} = 6.0 and 8.5 kcal/mol, respectively, compared to 1.1 kcal/mol for the formation of the AMPO-O₂ adduct in the presence of intramolecular H-bonding interaction.

This suggests that the favorability for O₂^{•-} addition toward nitrones is governed not only by the nucleophilic nature of this reaction but also by another factor. We suggest that the presence of intramolecular hydrogen bonding in the transition states would serve as an initial “anchor” for O₂^{•-}, thereby facilitating the O₂^{•-} addition to nitrones; this suggestion is in concert with our previous studies.^{32,46} An exception to this is DiMAPO which has the highest charge density on C-2 but only gave an intermediate rate of reactivity to O₂^{•-} with a calculated *k*_{rxn-1} of 3.52 × 10⁻² M⁻¹ s⁻¹ but gave the smallest endoergicity at the mPW1K level (see Table 1).

3.2.6. Effect of Full PCM Optimization and Single-Point PCM in DMSO and CH₃CN. So far, the PCM calculations were only performed via single-point energy computations. The effect of the dielectric constant during optimization of the TS structures was also considered to test if similar trends in the PCM energetics could be confirmed. Due to the computational cost associated with such methods, TS searches on O₂^{•-} adduct formation of AMPO and DMPO were performed at the PCM/B3LYP/6-31+G(d,p) level of theory (see Table 4). The calculated energetics and rate constants gave good correlations with

the calculated C-2 charge densities and are consistent with the predicted energetics using single-point PCM calculations, thereby further validating our results and earlier discussion.

In order to achieve a more accurate model for the calculation of the rate constants in a polar aprotic environment, PCM calculations were carried out using the solvents DMSO (ε = 47) and CH₃CN (ε = 37) which have comparable dielectric constants to that of DMF (ε = 38).⁶⁸ Shown in Table 6 are the thermodynamic data (Δ*H* and Δ*G*) and theoretical rate constants (*k*_{rxn-1}) for the formation of O₂^{•-} adducts calculated at the PCM(DMSO)/mPW1K and PCM(CH₃CN)/mPW1K levels. The qualitative trends in the calculated C-2 charges, Δ*G*[‡], Δ*G*_{rxn}, and *k*_{rxn-1} follow that at the PCM(H₂O)/mPW1K level.

3.3. Determination of Experimental Rate Constants.

3.3.1. UV-vis Stopped Flow Methodology. 3.3.1.1. General. There are conflicting reports in the literature concerning the magnitudes of the absolute rate constants of reaction of O₂^{•-} with various spin traps (see Table 5). This uncertainty greatly complicates the interpretation of spin-trapping experiments. The origin of the problem is based on the measurement of rate constants in the 10¹ to 10⁴ M⁻¹ s⁻¹ range using a competition-based method.³⁹ Such competitive kinetic approaches have become the standard route for rate constant determinations for several years and often employs poorly reproducible conditions, such as the use of radical generating systems with varying fluxes of O₂^{•-} and enzyme-based competitive species.^{30,39,40,42,43,45,46} In some cases, pulse radiolysis methods were also employed for rate constant determinations and do account for the trapping of O₂^{•-} but is best suited for measuring rate constants with magnitudes of 10⁶ to 10⁹ M⁻¹ s⁻¹.⁴¹ And, of course, many rate constants for O₂^{•-} addition are slower than this range.

3.3.1.2. Rate Law Determination. To avoid the problems typically encountered in the measurement of rate constants of O₂^{•-} trapping by nitrones, a more straightforward approach has been developed using UV-vis stopped-flow kinetics and using KO₂ as a direct source of O₂^{•-}, instead of the typical enzymatic O₂^{•-} generating systems. It is most convenient to monitor the progress of a reaction at a wavelength where one species, either a single reactant or product, is responsible for all of the observed absorbance. We have utilized phenol red as a probe molecule that generates a useful and convenient UV-vis signature during its reaction with O₂^{•-} in DMF. This reaction gave a broad transient absorbance in the visible region with a maximum at 575 nm (Figure 6, inset). Since the rate of formation of this new species at 575 nm is directly proportional to the kinetics of O₂^{•-} decay, in the presence of a spin trap as a competitive reactant, one can obtain the absolute rate constant (*k*₂) of the O₂^{•-} adduct's formation. The growth of the absorption signal (Figure 6) in the presence of phenol red and spin trap was fitted to an exponential function to yield an observed pseudo-first-order rate constant, *k*_{obsd} according to eq 3,

$$k_{\text{obsd}} = 1/\tau + k_1[\text{phenol red}] + k_2[\text{spin trap}] = \text{constant} + k_2[\text{spin trap}] \text{ (s}^{-1}\text{)} \quad (3)$$

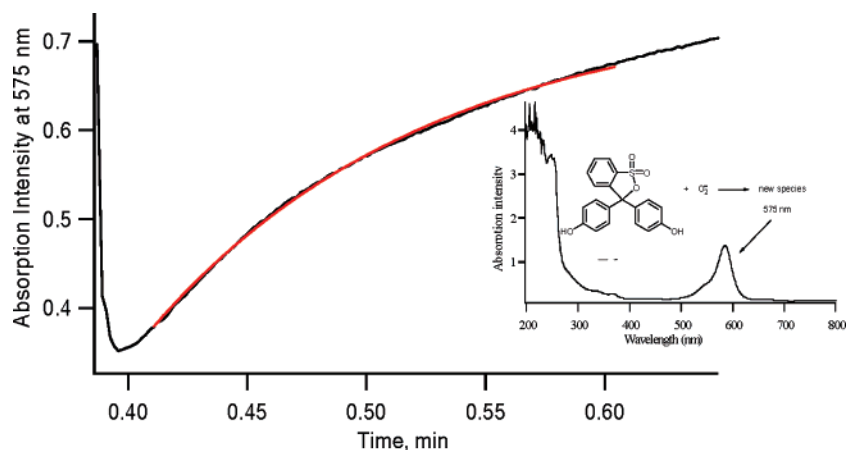
where τ is the lifetime of the O₂^{•-} in DMF/water solution, *k*₁ is the second-order rate constant for reaction of O₂^{•-} with phenol red, and *k*₂ is the second-order rate constant for reaction of O₂^{•-}

(68) PCM calculation using DMF is not implemented in the Gaussian 03 suite of programs; therefore, DMSO and CH₃CN were used instead.

Table 5. Survey of the Reported Apparent Rate Constants k_{app} ($M^{-1} s^{-1}$) for the Spin Trapping of Superoxide Radical by DMPO-Type Nitrones Using Various Methodologies (Technique Used, Competitor, Radical Generating System, and pH)

method	rate constants k_{app} ($M^{-1} s^{-1}$)				
	DMPO	DEPMPO	BocMPO ^a	EMPO	DEPO
I ⁴⁶ (EPR, SOD, light-riboflavin, pH 7.0)	n/a ^b	58	7	n/a	n/a
II ³⁹ (EPR, SOD, light-riboflavin, pH 8.0)	15.7	n/a	n/a	n/a	n/a
III ^{30,40} (EPR, DMPO, light-riboflavin, pH 7.0)	n/a	90 ^c	n/a	n/a	n/a
IV ^{38,43,44} (EPR, $O_2^{\bullet-}$ dismutation X/XO, pH 7.2)	2.0	3.95	3.45	10.9	31.1
V ⁴⁵ (EPR, ferricytochrome-c, X/XO, pH 7.0)	78.5 ± 2.1	n/a	77.0 ± 5.0	74.5 ± 6.4	n/a
VI ⁴² (EPR, $O_2^{\bullet-}$ dismutation, X/XO, pH 7.4)	2.4	0.53	0.24	n/a	n/a
VII ⁴¹ (pulse radiolysis, γ -irradiation of N_2O)	170 ± 40	n/a	<3	n/a	n/a
VIII ^d (UV-vis stopped-flow, phenol red, KO_2 , pH 10.5)	1.72 ± 0.01	0.65 ± 0.01	n/a	104.6 ± 4.6	n/a

^a 5-*tert*-Butoxycarbonyl-5 methyl-pyrroline *N*-oxide, also known as BMPO. ^b Not available. ^c Apparent rate constant is relative to $k_{2,DMPO} = 60 M^{-1} s^{-1}$. ^d This work.

**Figure 6.** Formation curve (black) measured at 575 nm following mixing of KO_2 solution with 625 μM AMPO and 500 μM phenol red solution and exponential curve fitting (red). The UV-vis spectrum for the mixture of 9 μM KO_2 and 9 μM phenol red solution is shown in the inset.

with the nitron spin trap. The complete rate law for eq 3 can be found in the Supporting Information (see p S13). The observed pseudo-first-order rate constant for the formation of the transient absorption (k_{obsd}), measured at short time scales, is linearly dependent (Figure S7) on the concentration of the spin trap at constant phenol red and $O_2^{\bullet-}$ concentrations. Therefore, with knowledge of the nitron's concentration, one can determine the second-order rate constant for *all* pathways that consume $O_2^{\bullet-}$ and are related to the concentration of the nitron.

3.3.1.3. Determination of Second-Order Rate Constants.

Table 6 shows the calculated absolute second-order rate constant

(k_2) obtained in 95:5 DMF/water solution. The order of increasing rate of reaction is as follows (k_2 in $M^{-1} s^{-1}$): DEPMPO < DMPO < EMPO < AMPO. The k_2 values for DMPO and DEPMPO using stopped-flow kinetics are also close to those found using Method VI (see Table 5) of 2.4 and 0.53 $M^{-1} s^{-1}$, respectively.⁴² These experimental rate constants follow the same qualitative trends for the calculated activation barrier in the aqueous phase at the mPW1K and B3LYP levels of theory (Table 1). The formation of the spin adducts were further confirmed by EPR spectroscopy as shown in Figure 7, and the resulting spectra show the formation of the $O_2^{\bullet-}$ adduct as the only paramagnetic product using the same experimental

Table 6. Calculated Relative Enthalpies ΔH (kcal/mol) and Free Energies ΔG (kcal/mol) as well as Rate Constants k_2 ($M^{-1} s^{-1}$) for the Formation of Various $O_2^{\bullet-}$ Adducts in DMSO at the PCM(DMSO)/mPW1K/6-31+G(d,p) and PCM(CH₃CN)/mPW1K/6-31+G(d,p) (in Parentheses) Levels of Theory at 298 K

spin trap (ST)	charge density (C-2)	enthalpies and free energies ^a								
		ST --- O ₂ ^{•-} ^b		[ST + O ₂ ^{•-}] ^c		ST-O ₂ ^{•-} ^d		k_{rxn-1} (calcd)	k_2^e (exptl)	k_2^f (exptl)
		$\Delta H_{complex}$	$\Delta G_{complex}$	ΔH^\ddagger	ΔG^\ddagger	ΔH_{rxn}	ΔG_{rxn}			
AMPO	0.053 (0.053)	-1.2 (-1.6)	7.5 (7.0)	6.9 (6.6)	18.1 (17.8)	-10.5 (-10.6)	1.2 (1.1)	10.2 (18.0)	134.7 ± 2.5	25.2 ± 1
EMPO	0.034 (0.034)	3.1 (2.5)	10.8 (10.5)	10.5 (10.0)	20.5 (20.0)	-4.8 (-5.1)	5.4 (5.1)	2.00 × 10 ⁻¹ (4.54 × 10 ⁻¹)	104.6 ± 4.6	10.9 ± 0.1
DMPO	0.012 (0.011)	3.7 (3.1)	11.0 (10.4)	14.2 (13.7)	24.1 (23.7)	-1.9 (-2.2)	8.9 (8.5)	8.71 × 10 ⁻⁴ (1.81 × 10 ⁻³)	1.72 ± 0.01	2.0 ± 0.2
DEPMPO	(0.036)	3.1 (0.036)	11.6 (11.2)	13.0 (12.7)	24.6 (24.3)	-3.7 (-4.0)	7.1 (6.9)	1.49 × 10 ⁻⁴ (2.65 × 10 ⁻⁴)	0.65 ± 0.01	4.0 ± 0.1
MCCP	n/a ^g	n/a	n/a	n/a	n/a	-3.5 (-4.1)	5.3 (4.7)	n/a	2.0 ± 0.03	n/a

^a Enthalpy, ΔH , and free energy, ΔG , values are all relative to the total ΔH and ΔG values of the ST and $O_2^{\bullet-}$ at infinite separation. ^b ST --- O₂^{•-} complex. ^c Transition state. ^d Products. ^e Experimental absolute second-order rate constants k_2 ($M^{-1} s^{-1}$) of reactions of various spin traps with $O_2^{\bullet-}$ in DMF-water (95%–5%) solution obtained by stopped-flow kinetics. ^f Experimental rate constants obtained using EPR technique and competition kinetics between spin trapping and spontaneous dismutation of $O_2^{\bullet-}$ as previously described.^{38,43} ^g Not available or applicable.

conditions used for the stopped-flow kinetics. However, the inconsistency found between the relative intensity of these spectra and observed rate constants cannot be explained based only on the half-lives of the $O_2^{\bullet-}$ adducts. The reported^{34,40,46,69} half-lives of $O_2^{\bullet-}$ adducts in H₂O are 14, 1, 10, and 8 min for DEPMPO, DMPO, EMPO, and AMPO, respectively, but these values may not follow a similar trend in the 95:5 DMF/water solvent system due to the difference in the mode of solvent–adduct interaction, solvent polarity, and pH. It has been reported⁷⁰ that the $O_2^{\bullet-}$ adducts are more stabilized in polar aprotic solvents such as in DMSO or DMF and that the half-life is shorter in a basic medium.

The predicted C-2 charge densities for EMPO and DEPMPO are almost the same, but the experimentally observed rate of $O_2^{\bullet-}$ addition with EMPO is faster than that with DEPMPO by 160-fold. One possible explanation for this could be that electrostatic interaction between the nitronyl-C and the $O_2^{\bullet-}$ unit plays a minor role in determining the rate of reaction on DEPMPO. Factors that could have affected the experimental rate constants as well as the calculated activation energy of $O_2^{\bullet-}$ addition to DEPMPO are the steric or repulsive nature of the bulky ethoxy substituents of the phosphoryl group.

3.3.1.4. Nature of 575 nm Absorption. Independent studies were performed to evaluate the nature of the carrier of the transient absorption at 575 nm. The 575 nm transient absorption was observed to be independent of pH (> 12) and indicates that the formation of the 575 nm peak is mediated by $O_2^{\bullet-}$. We also independently studied the reaction of $O_2^{\bullet-}$ with phenol (C₆H₅OH) so as to model one of the functional units in phenol red (see Figure 6 for its structure). The rate constant obtained for $O_2^{\bullet-}$ reaction with phenol using UV–vis stopped-flow kinetics was only 0.63 $M^{-1} s^{-1}$, significantly slower than the $O_2^{\bullet-}$ reaction with the EMPO and AMPO nitrones, and further indicates that H-abstraction alone of the phenolic-H by $O_2^{\bullet-}$ cannot compete with the $O_2^{\bullet-}$ addition reaction to an activated nitronyl, especially considering that the range of concentrations used for phenol red and nitrones are 0.5 mM and 0.3–120 mM (see Table S7), respectively. (We should note that there has

only been one measurement employing EPR spin-trapping of the reaction of $O_2^{\bullet-}$ with phenol and that the published rate constant was 5.8 × 10³ $M^{-1} s^{-1}$ in an aqueous system using xanthine–xanthine oxidase as the $O_2^{\bullet-}$ generating system.⁷¹)

3.3.1.5. Amide Group Reactivity to $O_2^{\bullet-}$. The high rate of reaction for AMPO with $O_2^{\bullet-}$ from both computational and experimental observations is very intriguing. AMPO not only exhibits high positive charge on the nitronyl-C compared to other spin traps, but the amide-H of AMPO also exhibits a strong intramolecular H-bonding interaction at the TS with $O_2^{\bullet-}$. Both effects could contribute significantly to the high rate of $O_2^{\bullet-}$ reaction with AMPO. The slight elongation of the N–H bond from 1.01 to 1.079 Å upon H-bonding to $O_2^{\bullet-}$ at the TS and finally to 1.54 Å for the AMPO–O₂ product formation are observed. To quantify this contribution to the calculated and observed rate constants for the formation of the AMPO–O₂^{•-} adduct, computational analysis and stopped-flow kinetic experiments for the reactivity of $O_2^{\bullet-}$ to the MCCP analogue were completed. A stopped-flow kinetic study for the reaction of $O_2^{\bullet-}$ to MCCP gave a reaction rate constant similar to that of DMPO and DEPMPO reactions to $O_2^{\bullet-}$ with $k_2 = 2.0 M^{-1} s^{-1}$. This rate constant can be accounted by the formation of a strong amide–O₂^{•-} complex. Our computational results (Table 6) show no indication of H-atom abstraction by $O_2^{\bullet-}$ of the amide-H, but the final product shows formation of a strong amide-H --- O–O H-bond of 1.55–1.57 Å (Figure 8). The $\Delta G_{rxn,298K}$ in DMSO is 5.3 kcal/mol which is more endoergic compared to the AMPO–O₂ adduct formation of $\Delta G_{rxn,298K} = 1.2$ kcal/mol in the same solvent. Although the observed rate constant of $k_2 = 2.0 M^{-1} s^{-1}$ for the $O_2^{\bullet-}$ addition to MCCP is a negligible contribution to the observed k_2 for $O_2^{\bullet-}$ addition to AMPO of 134.7 $M^{-1} s^{-1}$, the presence of amide-H --- O–O H-bond in the TS along with the high charge density on C-2 of AMPO does appear to facilitate the $O_2^{\bullet-}$ addition.

3.3.1.6. Ester Group Reactivity to $O_2^{\bullet-}$. The reactivity of $O_2^{\bullet-}$ to the carbonyl-C of an ester moiety was also investigated, although previous studies⁷² have shown that $O_2^{\bullet-}$ addition to

(69) Stolze, K.; Udilova, N.; Rosenau, T.; Hofinger, A.; Nohl, H. *Biol. Chem.* **2003**, *384*, 493–500.

(70) Barbat, S.; Clement, J. L.; Olive, G.; Roubaud, V.; Tuccio, B.; Tordo, P. In *Free Radicals in Biology, Environment*; Minisci, F., Ed.; Kluwer Academic Publishers: Dordrecht, The Netherlands, 1997; pp 39–47.

(71) Yasuhisa, T.; Hideki, H.; Muneyoshi, Y. *Intl. J. Biochem.* **1993**, *25*, 491–4.

(72) Gibian, M. J.; Sawyer, D. T.; Ungermann, T.; Tangpoonpholvivat, R.; Morrison, M. M. *J. Am. Chem. Soc.* **1979**, *101*, 640–644. San Filippo, J. J.; Chern, C.-I.; Valentine, J. S. V. *J. Org. Chem.* **1976**, *41*, 1077–1078.

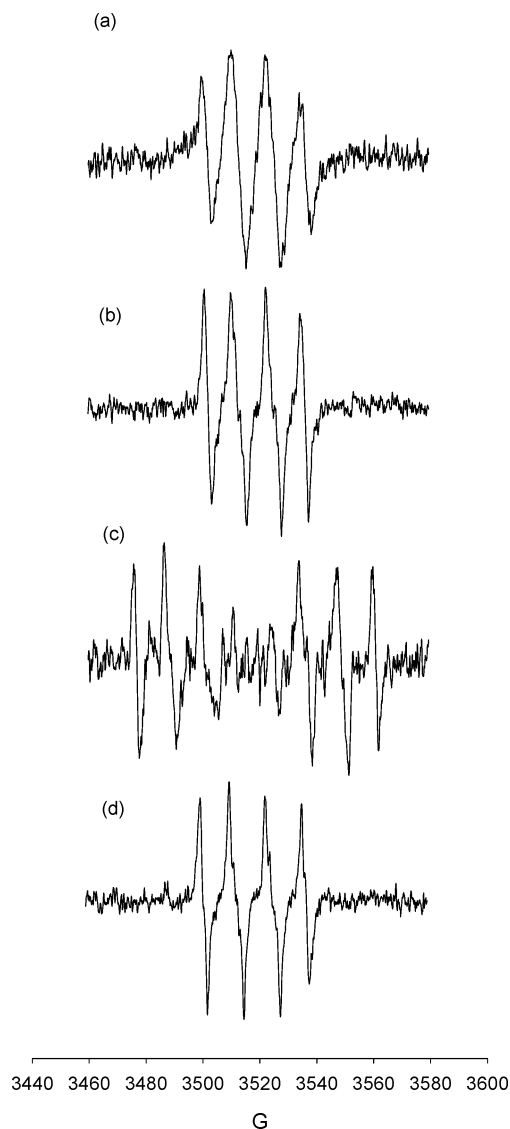


Figure 7. X-band EPR spectra of various superoxide radical anion adducts of (a) 250 mM AMPO (I, 89%: LW = 1.76 G, a_N = 12.61 G, $a_{\beta-H}$ = 9.95, $a_{\gamma-H}$ = 1.56 G; II, 11%: LW = 1.41 G, a_N = 11.15 G, $a_{\beta-H}$ = 8.30 G, $a_{\gamma-H}$ = 0.62 G); (b) 210 mM EMPO (I, 58.6%: LW = 1.4 G, a_N = 12.2 G, $a_{\beta-H}$ = 7.7 G; II, 41.4%: a_N = 12.3 G, $a_{\beta-H}$ = 10.5 G); (c) 205 mM DEPMPO (I, 48.8%: LW = 0.55 G, a_N = 12.3 G, $a_{\beta-H}$ = 10.3 G, $a_{\gamma-H}$ = 1.1, $a_{\gamma-H}$ = 0.5 G, a_P = 48.6 G; II, 51.2%: LW = 1 G, a_N = 13.4 G, $a_{\beta-H}$ = 11.0 G, $a_{\gamma-H}$ = 0.6, $a_{\gamma-H}$ = 0.5 G, a_P = 47.2 G); and (d) 240 mM DMPO (I, 57.2%: LW = 0.78 G, a_N = 12.8 G, $a_{\beta-H}$ = 10.1 G, $a_{\gamma-H}$ = 1.4 G; II, 42.8%: LW = 1.7 G, a_N = 12.9 G, $a_{\beta-H}$ = 11.7 G, $a_{\gamma-H}$ = 2.1 G) in 5% water–95% DMF solution with saturated KO_2 . Spectrometric setting: scan range, 120 G; MA, 0.5 G; MF, 100 kHz; TC, 81.9 ms; RG, 3.5×10^5 ; MW power, 19.85 mW. (See Figure S1 of the Supporting Information for the simulated spectra.)

esters results in its hydrolysis to the resulting carboxylic acid. The reactivity of ethyl trimethylacetate (ethyl pivalate) to $O_2^{\bullet-}$ was studied by the stopped-flow method using the same experimental conditions employed above to investigate if the addition of $O_2^{\bullet-}$ to the pivalate's ester group contributed to the high rate constant observed for EMPO. Results show no change in the k_{obsd} even at a very high ester concentration of 240 mM and suggest that the ester group is inert toward $O_2^{\bullet-}$. Computationally, the addition of $O_2^{\bullet-}$ to the carbonyl-C in ethyl pivalate gave an endoergic reaction of about $\Delta G_{rxn,aq} = 13.7$ kcal/mol at the B3LYP level.

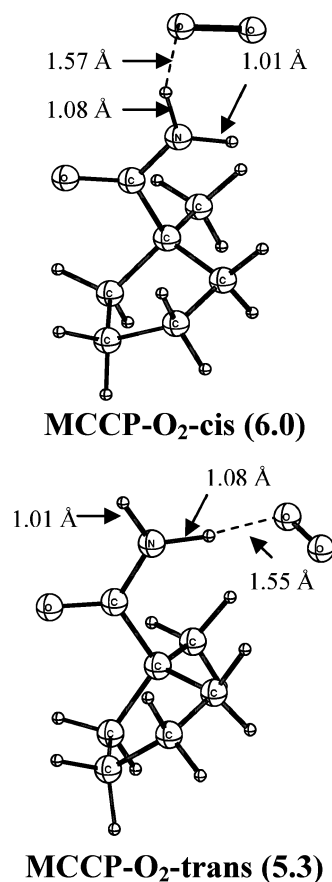


Figure 8. Structures of $O_2^{\bullet-}$ complex with MCCP showing the free energies of complex formation in DMSO in kcal/mol at the mPW1K/6-31+G(d,p) level of theory at 298 K. See Table 6 for the relative free energies and enthalpies of formation of the most stable complex.

3.3.2. Competitive Kinetics by EPR Methods.

3.3.2.1. Determination of Second-Order Rate Constants.

An alternative method was carried out to further confirm the trends observed for the reactivity of various nitrones to $O_2^{\bullet-}$ as derived by the UV–vis stopped-flow kinetic procedure. Using the EPR spectroscopic technique, rate constants were determined based on the competition between the $O_2^{\bullet-}$ trapping by a nitron and the spontaneous dismutation of $O_2^{\bullet-}$ in aqueous media. As demonstrated from previous works by Tuccio and co-workers,^{38,43} the kinetic curves are obtained after treatment of these spectra using both singular value decomposition (SVD) and pseudo-inverse deconvolution methods. This method for rate constant determination also eliminates the effect of a varying flux of $O_2^{\bullet-}$ production as commonly encountered in previous studies based on the competition with $O_2^{\bullet-}$ scavengers.^{30,39,45,46,73} Using the same EPR experimental technique previously employed,^{38,43} AMPO gave the highest k_2 value as compared to EMPO, DEPMPO, and DMPO (Table 6). The general trend in the rate constant is consistent to that observed using the UV–vis stopped-flow method with the exception of DMPO and DEPMPO in which the rate constant is higher for DMPO than for DEPMPO using EPR.

3.3.2.2. Discrepancy between Theoretical and Experimental Rate Constants.

Computational predictions of absolute rate

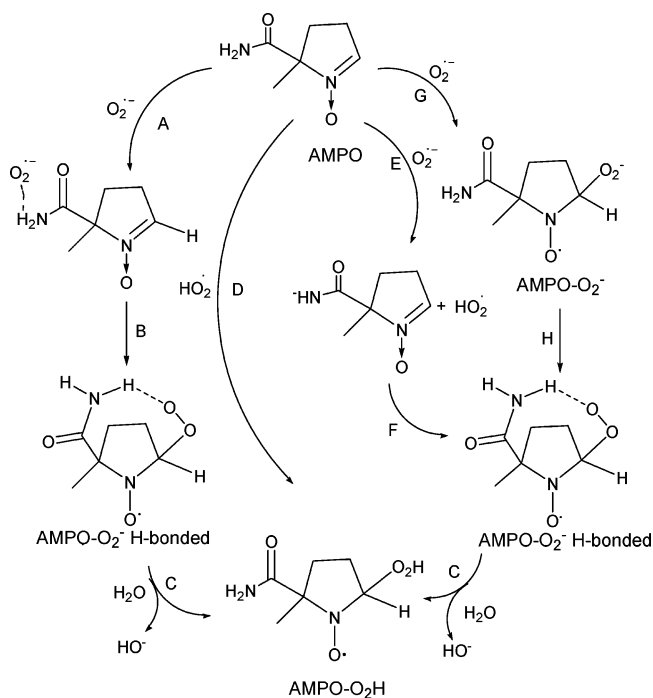
(73) Finkelstein, E.; Rosen, G. M.; Rauckman, E. J. *Mol. Pharmacol.* **1979**, *16*, 676–685. Rosen, G. M.; Tsai, P.; Weaver, J.; Porasuphatana, S.; Roman, L. J.; Starkov, A. A.; Fiskum, G.; Pou, S. *J. Biol. Chem.* **2002**, *277*, 40275–40280.

constants is a challenging process and requires very accurate predictions of the activation barriers and often complete consideration of dynamic effects and the shape (curvature) of the potential energy surface near the transition state. In this study, tunneling has been parametrized via Wigner tunneling corrections, and we have only utilized DFT methods for the energetic evaluations, primarily because of the diverse nature and the significant size of these chemical systems. We do anticipate some error in the computational rate constants due to the effects that we are neglecting; however, qualitative trends between different nitrones should be reproduced.

The observed k_2 values for AMPO and EMPO using the EPR SVD-deconvolution method are significantly lower compared to the UV-vis stopped-flow method, and this could be due to the following reasons. (1) The use of SVD-deconvolution kinetics only monitors the rate of formation of the nitron- $O_2^{\bullet-}$ adduct by EPR, while the UV-vis stopped-flow method monitors the rate of $O_2^{\bullet-}$ decay that depends on the nitron's concentration. The reactivity of $O_2^{\bullet-}$ to the amido group without the nitron functionality using MCCC only gave negligible contribution to the observed rate constant using stopped-flow kinetics. (2) Since simultaneous spin-adduct formation and decay occur during spin trapping, the EPR technique could not account for the $O_2^{\bullet-}$ adducts that decomposed during spin adduct formation while the UV-vis stopped-flow technique accounts for all of the reactions which deplete the concentration of $O_2^{\bullet-}$ and which depend on the nitron's concentration. (3) Using the EPR SVD-deconvolution kinetics, the reaction of both HO_2^{\bullet} and $O_2^{\bullet-}$ were considered, while the stopped-flow method only considers the reaction of the $O_2^{\bullet-}$ species. It has been shown⁷⁴ that HO_2^{\bullet} and $O_2^{\bullet-}$ exhibit high reactivity with the relatively more stable nitroxides such as 2,2,6,6-tetramethylpiperidinoxyl (TPO) and 3-carbamoyl-2,2,5,5-tetramethylpyrrolidinoxyl (3-CP) than the DMPO-OOH adduct. The bimolecular rate constant for the reaction of TPO and 3-CP with HO_2^{\bullet} is on the order of 10^6 – 10^8 $M^{-1} s^{-1}$ and is lower than that with $O_2^{\bullet-}$ ($k_2 \sim 10^3$ $M^{-1} s^{-1}$). Therefore, it follows that by monitoring the formation of DMPO-OOH alone, one can neglect the contribution of the spin adduct decomposition by HO_2^{\bullet} and $O_2^{\bullet-}$. (4) Solvent effects can significantly affect the rate of adduct formation and adduct stability as discussed above.

3.3.3. Thermodynamics of AMPO- O_2H Formation. To further interpret the reaction energies obtained for the formation of the $O_2^{\bullet-}$ adduct of AMPO at neutral pH, four possible scenarios were considered as shown in Scheme 2: (1) initial $O_2^{\bullet-}$ complexation to the amide-H (Reaction A); (2) addition of protonated $O_2^{\bullet-}$ (Reaction D); (3) H-atom abstraction of the amide-H from AMPO (Reaction E); or (4) direct addition to the nitronyl-C of AMPO in the absence of intramolecular H-bonding (Reaction G). Free energies of reaction at the B3LYP level show that Reactions A and G are the most preferred with $\Delta G_{rxn,298K}$ values in the aqueous phase of 8.6 and 3.8 kcal/mol, respectively, compared to the formation of HO_2^{\bullet} from $O_2^{\bullet-}$ and water or from H^+ abstraction of the amide-H by $O_2^{\bullet-}$ with $\Delta G_{rxn,298K} = 27.4$ and 20.5 kcal/mol, respectively. Due to the IEF-PCM solvation method employed in this work (i.e., using Gaussian 03), the energy values previously reported³⁴ using

Scheme 2. Pathways for the Formation of the AMPO- O_2H Adduct^a



^a The reaction free energies in the aqueous phase ($\Delta G_{rxn,298K}$) in kcal/mol at the PCM(water)/B3LYP/6-31+G(d,p)//B3LYP/6-31G(d) level are for reactions A (8.6), B (-2.9), C (14.7), D (-6.9), E (20.5), F (-14.8), G (3.8), and H (1.9).

Gaussian 98⁷⁵ are slightly different by about 0.1 to 2.3 kcal/mol for Reactions D, E, F, and G with $\Delta G_{rxn,aq,298K}$ values of -7.0, 19.4, -13.7, and 6.2 kcal/mol, respectively.

In this study, we demonstrated that the formation of AMPO- $O_2^{\bullet-}$ with intramolecular H-bonding could also be favored via initial complexation of $O_2^{\bullet-}$ to the amide-H (Reaction A). In fact, the formation of AMPO- $O_2^{\bullet-}$ via Reaction A is exoergic, with $\Delta G_{rxn,298K} = -2.9$ kcal/mol compared to the formation of AMPO- $O_2^{\bullet-}$ from the non-hydrogen-bonded AMPO- $O_2^{\bullet-}$ adduct with $\Delta G_{rxn,298K} = 1.9$ kcal/mol (Reaction H). The $\Delta G_{rxn,298K}$ calculated for Reaction H of 1.9 kcal/mol is different from our previously reported³⁴ value of $\Delta G_{rxn,298K} = -12.2$ kcal/mol. The discrepancy in $\Delta G_{rxn,298K}$ values reported for Reaction H is due to the difference in the calculated PCM energies using Gaussian 98 versus Gaussian 03, in which the former did not give the same qualitative trend in PCM free energies as that in the gas phase; therefore, a different conformer was considered for the calculation of Reaction H from our previous study.³⁴ However, if one uses the same conformer that was used in this work, the $\Delta G_{rxn,298K}$ value would have been 1.1 kcal/mol endoergic which is closer in value to what have been predicted for Reaction H in this work. The free energy value of 1.9 kcal/mol for Reaction H is more consistent with our calculated pK_a for AMPO of 21.7 (comparable to the reported typical pK_a for alkanamides (RC(=O)NH₂) of 25;⁷⁶ see previous work) and that of ROOH of 11.65–12.8⁷⁷ which would indicate that the equilibrium should favor the reactants over the products.

(75) Frisch, M. J., et al. *Gaussian 98*, revision A.11.3 ed.; Gaussian, Inc.: Pittsburgh, PA, 2002.

(76) Gordon, A. J.; Ford, R. A. *The Chemist's Companion: A Handbook of Practical Data, Techniques, and References*; Wiley-Interscience: New York, 1972.

(77) Richardson, W. H.; Hodge, V. F. *J. Org. Chem.* **1970**, *35*, 4012–4016.

(74) Goldstein, S.; Merenyi, G.; Russo, A.; Samuni, A. *J. Am. Chem. Soc.* **2003**, *125*, 789–795.

Moreover, according to Reaction C, the protonation of H-bonded or non-H-bonded AMPO- $O_2^{\bullet-}$ by H_2O to form the final product, AMPO-OOH, is endoergic by $\Delta G_{rxn,298K} = 14.7$ or 16.7 kcal/mol, respectively. However, Reaction C gave a significant discrepancy between Gaussian 98 and 03 with a $\Delta G_{rxn,aq,298K}$ difference of 26.9 kcal/mol, the former being more exoergic, and this is due to the difference of 20.1 kcal/mol between the two Gaussian versions for the calculated solution total free energy (with all nonelectrostatic terms) of the charge-dense hydroxide anion. Therefore, a plausible pathway for the formation of the AMPO-OOH adduct, based on thermodynamic and kinetic considerations, is via the $A \rightarrow B \rightarrow C$ reaction path as presented in Scheme 2 with an endoergic total $\Delta G_{rxn,295K}$ for AMPO-OOH formation at neutral pH of 20.3 kcal/mol and is exoergic by -6.9 kcal/mol under acidic conditions (Reaction D).

4. Conclusions

This study suggests the use of AMPO, CPCOMPO, TFMPO, and *N*-monoalkylamide-substituted nitrones such as MAMPO and EMAPO as a potential new family of nitrones with improved efficiency for $O_2^{\bullet-}$ trapping. The use *N*-monoalkylamide substituents as a linker group offers advantages over alkyl ester substituents as amides are not susceptible to hydrolysis in the presence of intracellular esterases, and their potential for molecular tethering offers several possibilities for improving adduct stability and target specificity in cellular systems. We have shown that the positive charge on the nitronyl-carbon (the site of $O_2^{\bullet-}$ attack) along with the presence of intramolecular H-bonding interactions in the TS facilitate the early transition state and the rate of $O_2^{\bullet-}$ adduct formation. A new stopped-flow UV-vis kinetic method as well as EPR-based competition kinetics gave rate constant values that are highest for AMPO, followed by EMPO, and with DEPMPO and DMPO having the

slowest reactivity. The strong N-H... $O_2^{\bullet-}$ interaction in the transition state predicted for monosubstituted *N*-alkylamide nitrones was confirmed by stopped-flow kinetics and appears to play a crucial role in facilitating the $O_2^{\bullet-}$ adduct formation.

Moreover, this new insight on $O_2^{\bullet-}$ reactivity may have significant ramifications in the initiation of oxidative damage in protein systems in which the amide-H can play a role in the catalysis and selectivity of hydroperoxide formation. It has been shown that hydroperoxide formation in some peptides is favored in the presence of amino substituents, and we hypothesize that this selective reaction could be mediated by the formation of amino-H... $O_2^{\bullet-}$ interactions.⁷⁸ This aspect of possible amide-H (or amino-H) mediated hydroperoxide formation in peptide systems is now being investigated in our laboratory.

Acknowledgment. NIH Grant HL81248 is acknowledged for support of this work. J.L.Z. acknowledges support from NIH Grants HL38324, HL63744, and HL65608. C.M.H. also acknowledges support from the NSF-funded Environmental Molecular Science Institute (CHE-0089147). The Ohio Supercomputer Center (OSC) is acknowledged for generous computational support of this research. Thanks to Prof. Matthew S. Platz of the Ohio State University for helpful suggestions. Special thanks to Dr. B. T. S. Thirumamagal for the synthesis of EMPO and AMPO.

Supporting Information Available: Energies, enthalpies, free energies, Cartesian coordinates for all spin traps and their corresponding spin adducts are available as Supporting Information, as well as the complete citation for refs 52 and 71. This information is available free of charge at <http://pubs.acs.org>.

JA0702622

(78) Winterbourn, C. C.; Parsons-Mair, H. N.; Gebicki, S.; Gebicki, J. M.; Davies, M. J. *Biochem. J.* **2004**, *381*, 241–248.